UNIVERSITY OF BIRMINGHAM

**School of Chemistry**

# Exploiting the Instability of Capped Metal Nanoparticles on Metallic Surfaces

Nashwa Awais

**Project Supervisors: Professor Tim Albrecht, Dr Paramaconi Rodriguez**

Submitted for the degree of

**MSc by Research**

UNIVERSITY OF
BIRMINGHAM

## University of Birmingham Research Archive

### e-theses repository

This unpublished thesis/dissertation is copyright of the author and/or third parties. The intellectual property rights of the author or third parties in respect of this work are as defined by The Copyright Designs and Patents Act 1988 or as modified by any successor legislation.

Any use made of information contained in this thesis/dissertation must be in accordance with that legislation and must be properly acknowledged. Further distribution or reproduction in any format is prohibited without the permission of the copyright holder.

# Acknowledgement

I would firstly like to thank both my supervisors, Professor Tim Albrecht and Dr Paramaconi Rodriguez, for their continued support and encouragement. I began this degree with very limited experience and am truly grateful for the opportunity and guidance they have both afforded me throughout my project.

I would also like to thank the members of both research groups, particularly Dr Anton Vladyka and Matthew Lawrence for their training and assistance with experimental work.

Last but not least, a massive thank you goes to my family, for their unwavering support and encouragement from the moment I decided to apply.

## Abstract

Small metal nanoparticles (NPs) within the size range of 1-3 nm exhibit unique electronic and catalytic properties. Thiolated nanoparticles have been shown to undergo an at least partly entropically driven redistribution of the capping layer when AuNPs are exposed to bare Au substrates. It has been postulated that different substrate and NP materials may be employed for surface design, as the interaction between the protected nanoparticles with the metal substrate could aid in the removal of the thiol layer.

The aim of this work was to investigate outcomes of surface structure modification for different substrate-NP combinations, in alkaline media and via their performance in the electro-catalytic decomposition of glycerol (GlyOH). Pt surface/AuNP and Au surface/PtNP combinations were investigated, by immersion of the surfaces into solutions of the NPs.

Au NPs were synthesised using a bottom-up metal reduction, and Pt NPs were synthesised via the cathodic corrosion method. Electrochemical responses were measured using cyclic voltammetry (CV). Addition of the Au NPs to the Pt surface resulted in a lower current response, but no change in characteristic Pt peaks within the CV profile, nor emergence of Au related features, indicate that the Au NPs remain protected on the surface. However, addition of the Pt NPs to the Au surface resulted in a notable change in the CV profile, to include both Au and Pt characteristic peaks. In particular, the effect of modifying the Au surface with PtNPs was significant, in that the characteristic peak corresponding to the electro-oxidation of GlyOH by Pt became visible. These findings are in line with a potential thiol redistribution effect, as shown for the Au surface/AuNP system, although further investigation into the surface dynamics of the nanoparticles on the surface may be required.

# Contents

Acknowledgement ..... i

Abstract ..... ii

List of Abbreviations ..... v

1. Introduction ..... 1

1.1 Catalysis ..... 2

1.2 Nanomaterials in Catalysis ..... 3

2. Nanoparticles ..... 5

2.1 Gold ..... 5

2.2 Platinum ..... 6

2.3 Thiols on Metal Surfaces ..... 9

2.4 Synthesis of Nanoparticles ..... 10

2.4.1 Dry Synthesis ..... 10

2.4.2 Wet Synthesis ..... 10

2.5 Physical Characterisation Techniques ..... 14

2.5.1 UV-Vis Spectroscopy ..... 14

2.5.2 Transmission Electron Microscopy (TEM) ..... 15

2.6 Electrochemical Characterisation ..... 15

2.6.1 Cyclic Voltammetry ..... 16

3. Experimental ..... 18

3.1 Glassware Cleaning Procedures ..... 18

3.1.1 Nanoparticle Synthesis ..... 18

3.1.2 Electrochemistry ..... 18

3.2 Au NP Synthesis ..... 18

3.2.1 Characterisation ..... 19

3.3 Pt NP Synthesis ..... 19
3.4 Electrochemistry ..... 20
4. Results and Discussion ..... 22
4.1 Au NP Synthesis ..... 22
4.1.1 UV-Vis Spectroscopy ..... 22
4.1.2 TEM Imaging ..... 23
4.2 Pt NP Synthesis ..... 23
4.2.1 Synthetic Procedure ..... 23
4.2.2 TEM Imaging ..... 24
5. Electrochemistry of Au and Pt NPs in 0.1 M NaOH ..... 25
5.1 Au Electrode Surface ..... 25
5.2 Pt Electrode Surface ..... 26
5.3 NPs on Au and Pt Electrode Surfaces ..... 27
5.3.1 Au surface/PtNP ..... 27
5.4 Conclusions ..... 30
6. Electrochemistry of Au and Pt NPs in 0.1 M Glycerol ..... 32
6.1 Introduction ..... 32
6.2 Au Electrode Response ..... 34
6.3 Pt Electrode Response ..... 35
6.4 NPs on Electrode Surfaces ..... 35
6.4.1 Au surface/PtNP ..... 35
6.4.2 Pt surface/AuNP ..... 40
6.5 Conclusion ..... 42
7. References ..... 44

# List of Abbreviations

| | |
|---|---|
| **NP** | Nanoparticle |
| **SR** | Thiol group (R: organic component) |
| **GlyOH** | Glycerol |
| **CV** | Cyclic voltammetry |
| **STM** | Scanning tunnelling microscopy |
| **MNP** | Metallic nanoparticle |
| **SPR** | Surface plasmon resonance |
| **PGM** | Platinum group metal |
| **SAM** | Self-assembled monolayer |
| **AC** | Alternating current |
| **TEM** | Transmission electron microscopy |
| **WE** | Working electrode |
| **CE** | Counter electrode |
| **RE** | Reference electrode |
| **SCE** | Saturated calomel electrode |
| **RHE** | Reversible hydrogen electrode |

# 1. Introduction

As the global population continues to rise, the world faces ever increasing pressure to meet energy demands in a responsible, sustainable manner. Recent scientific investigations have explored the employment of functionalised catalysts, whose design and catalytic efficiency may provide advances in the fields of energy conversion, sensing, and medicine, among others.[1–5]

Metallic nanomaterials with a size range between 1 and 10 nm have been of great scientific interest in this context. These materials possess unique electronic and catalytic properties, as their properties often lie between those of bulk and molecular systems.[6] Showing considerable potential as catalysts with greater selectivity and activity, nanoclusters have become important in the field of catalysis research, in particular when immobilised onto support electrodes.[7]

The low availability and high cost of the metals often used in catalysis (Au, Pt, Pd) require a compromise between maximising catalytic efficiency, while also keeping particle loading to a minimum. Catalytic surfaces containing different active materials are capable of catalysing multiple reactions due to their differing selectivity, giving increased efficiency and applicability of a single catalytic surface. In the case of small metal nanoparticles, their long-term uses are limited due to their instability.[8] Stabilised nanoparticles, protected via a thiol capping layer, may therefore provide a route for surface modification of metallic surfaces. Notably, in a previous study, gold nanoparticles (Au NPs) were immobilised onto an Au (111) substrate, but shown to be structurally unstable, as shown by electrochemical methods and (electrochemical) Scanning Tunnelling Microscopy (STM). This was at least in part due to the dynamic nature of the Au/thiol bond, which lead to the re-distribution of the capping layer and hence the destabilisation of the particle core. The resulting 'islands' offered a new avenue towards the modification of substrate surfaces, especially when considering the combination of different NP and substrate materials. [6]

Accordingly, in this thesis, thiolated Au and Pt nanoparticles were synthesised, characterised and employed for the surface modification of Au and Pt micro-electrodes. The aim of the project was to gain insight into the potential of thiolated nanoparticles for modification of surfaces, by observing if the interaction between the thiol-protected nanoparticles and a

metal electrode could aid in the removal of their capping layer and hence enhance their surface activity. In order to test the success of the surface modification process, for example whether elemental Pt or Au had been exposed on the surface, specific catalytic reactions were employed. This included the electrocatalytic decomposition of glycerol in alkaline media, which occurs at different electrode potentials for the two substrates.

## 1.1 Catalysis

A catalyst provides a reaction pathway with a lower activation energy barrier, without being consumed in the process, and therefore remains unaltered for re-use. Attractive properties of catalysts include stability, high activity and good selectivity.[9]

Catalysts can be divided into two major categories: heterogeneous and homogeneous. Homogeneous catalysts are in the same phase as the reactants in the system, *e.g.* sulfuric acid ($H_2SO_4$) as a catalyst in the nitration of benzene, and are generally soluble complexes with all their catalytic sites accessible.[10] Though they provide greater selectivity, their separation from the end products can be challenging.[11] Heterogeneous catalysis is therefore preferred in some cases, with catalysts generally immobilised onto support surfaces such as silica, or other materials that allow for efficient anchoring of catalytic compounds.[12]

Conceptually, in heterogeneous catalysis, the process can be broken down into four steps:

1) diffusion of the species toward the electrode
2) adsorption of the target reactant on the catalytic surface
3) the reaction itself and formation of intermediate species
4) desorption of products

Though the catalyst is required to interact with and activate reactants, the interaction between the catalytic material and adsorbates, including intermediates or products, should neither be too strong or too weak, according to the Sabatier principle.[13] Too weak an interaction means the adsorbate will not bind effectively to the catalyst, resulting in poor turnover. Too strong an interaction leads to the blockage of active sites, preventing the reaction from proceeding and to poisoning of the catalyst.[1]

First conceptually introduced by Taylor *et. al*.[14], active sites are the points on a surface that directly catalyse a reaction.[15] The nature of the catalytic surface and its active sites therefore have an impact on its performance.

## 1.2 Nanomaterials in Catalysis

In metallic nanomaterials, the electrons of the metal atoms are confined to molecular dimensions, leading to unusual and unique properties, including small energy gaps and high catalytic activity.[16] The latter is due to a large number of exposed surface atoms, with low coordination numbers, that may easily be varied by tuning the nanoparticle size.[17] Metallic nanoparticles (MNPs) are therefore attractive in the field of catalysis, with materials of focus being Au, Pt and Rh.[9] Au in particular has been a material of choice for oxidation catalysis, and was shown to exhibit size-correlated activity towards the oxidation of carbon monoxide, with sub-nanometre sized NPs showing high catalytic activities.[18,19]

Expenses attached with the employment of precious metals in catalytic systems mean improvements in their efficiency are highly desirable. In this respect, alloying metals gives advantages over the use of single-metal catalysts in that:

- Alloying of metals leads to decreased loading of each metal, potentially reducing the costs of each while maintaining a high catalytic activity.

- Interactions between the metals can alter their electronic and structural properties, changing their catalytic performance further.

Some alloyed NPs have been reported to have enhanced catalytic activity and selectivity, as compared to their individual elemental NPs, as they may be tuned via variation of composition and cluster morphology.[8] Another aspect could be the potential to overcome issues such as poisoning of catalyst surfaces, a result of contamination of active sites.[9,20,21] An example is platinum, used in a number of catalytic processes due to its catalytic activity and stability.[22] It is used to catalyse the methanol electro-oxidation reaction (MOR) in direct fuel cells, but becomes poisoned due to its high affinity towards carbon monoxide (CO) intermediates, which deactivate the platinum.[23] Alloying of the platinum with other noble metals *i.e.* Rh and Ir has been shown to decrease the extent of the surface poisoning, and Au has been shown to improve the MOR turnover, as it has a weak CO binding energy.[24] Combinations of Au-Pt alloy catalysts have shown efficiency toward the oxygen reduction

reaction (ORR), as well as electro-catalytic decomposition of organic compounds such as methanol and formic acid.[24–26] Further, tuning the composition of Au-Pt alloy electrocatalysts has revealed a correlation between the surface composition and its catalytic activity, providing a route towards optimisation of such surfaces.[27]

## 2. Nanoparticles

Nanoparticles (NPs) are materials with a size range of between 1 and 100 nm, and can be classified based upon their composition, size and shape.[28] There are a variety of NPs of interest, including metallic, polymeric and ceramic,[29] with the focus of this project being on metallic NPs (MNPs).

MNP surfaces can be passivated via coordination with a 'capping layer', which typically consists of surfactants, thiols or other ligands, resulting in an enhanced stability. [2,30] One such example of stabilised nanoparticles is monolayer protected nanoparticles, in which a metallic core is protected and stabilised by a 'capping layer' of a thiol species *e.g.* R-SH.[31] In these systems, the size of the NP core can be tuned from 1.5 to 8 nm and the capping layer offers further opportunities for surface functionalisation. [2,32]

### 2.1 Gold

Gold nanoparticles have been of particular scientific interest due to the prominent optical resonance they exhibit in the visible region, their electronic properties and the sensitivity of this behaviour towards their morphology.[33] Their surface properties, *e.g.* surface plasmon resonance (SPR) have shown their potential application as labels for cancerous cells, among other imaging and sensing tools.[32,34] Gold NPs can be prepared with various core diameters, though a region of interest remains between 1-3 nm.[6]

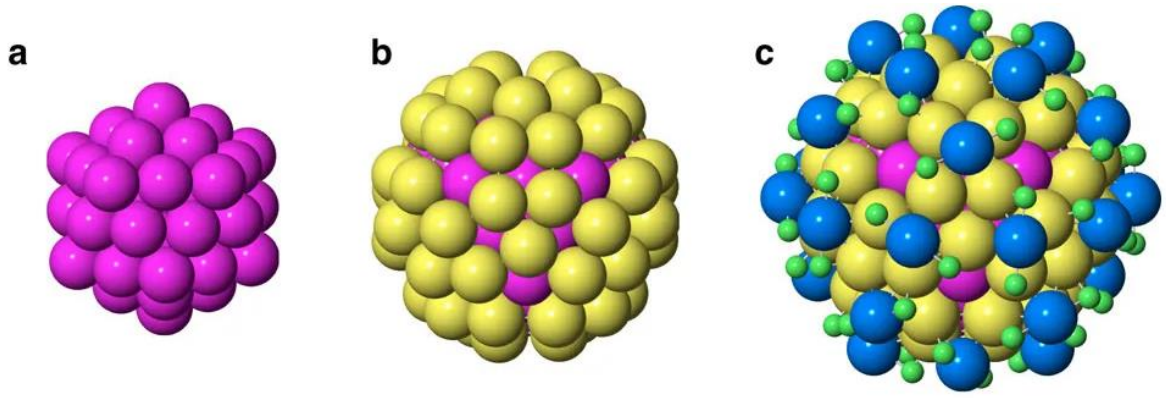


*Figure 1 Generated structure of an $Au_{144}(SR)_{60}$ cluster (R being the organic component of the thiol). (**a**) icosahedral gold core of 54 atoms (**b**) initial icosahedral core surrounded by a further 60 gold atoms, giving the "grand core" (**c**) Au core surrounded by green sulfur atoms in a staple structure arrangement, with blue representing the Au atoms in the SR-Au-SR surface structure. Adapted with permission, Kirsten M.Ø. Jensen et al, Nat. Commun., 2016, 7, 11859. Copyright 2016, Springer Nature.*

Generally, thiolated gold NPs are atomically precise, with a metallic core, which is surrounded by the thiol capping layer in a "staple" structure arrangement that varies among systems of different core sizes, for example the SR-Au-SR arrangement as found in $Au_{144}(SR)_{60}$, while $Au_{25}(SR)_{18}$ features a stoichiometry of SR-Au-(SR)-Au-SR, and more simple staples of -Au-S-Au- are found on $Au_{102}(SR)_{44}$.[35–37]

Thiol protected gold clusters have been extensively studied, with a prominent example being $Au_{144}(SR)_{60}$, as shown in Figure 1. This thiolated nanocluster was the first to display unique electronic features due to its size, being a bridge between molecules and cluster systems,[38,39] as it lies in a region between that of small nanoparticle systems *e.g.* $Au_{25}(SR)_{18}$, and larger Au particles that begin to exhibit surface plasmons.[40]

## 2.2 Platinum

Platinum is a transition metal, classified along with palladium, rhodium, ruthenium, osmium and iridium as among the platinum group metals (PGMs), due to their similar chemical and physical properties.[41] These elements are efficient electrocatalysts, as well as possessing desirable properties of thermal stability and resistance to corrosion.[42]

Platinum is a rare and expensive resource, due in part to the difficulty of purification as its ores often contain other PGMs, which require an intricate method of extraction.[43] Platinum dissolves upon immersion in aqua regia, a mixture of hydrochloric (HCl) and nitric acid ($HNO_3$), to give chloroplatinic acid ($H_2PtCl_6$), commonly used as a precursor in the synthesis of Pt NPs. As mentioned previously, it faces limitations in its poisoning and deactivation by certain substances, and high costs. Despite this, it is used in fuel cells and catalytic converters in industry, with excellent catalytic properties not matched by elements outside of the PMG-noble metal classification.[29,41]

Platinum NPs have been investigated with regards to their degradation mechanisms, with four primary approaches being: (i) agglomeration, (ii) Ostwald ripening, (iii) dissolution and (iv) detachment of the particles from a support electrode. Of the four processes, the former two can be considered as associative mechanisms, and the latter two dissociative.[44] These mechanisms have been explored using supported Pt electrocatalyst, a diagrammatic representation of which is presented in Figure 2 (adapted from Shao-Horn *et. al.*[45]).

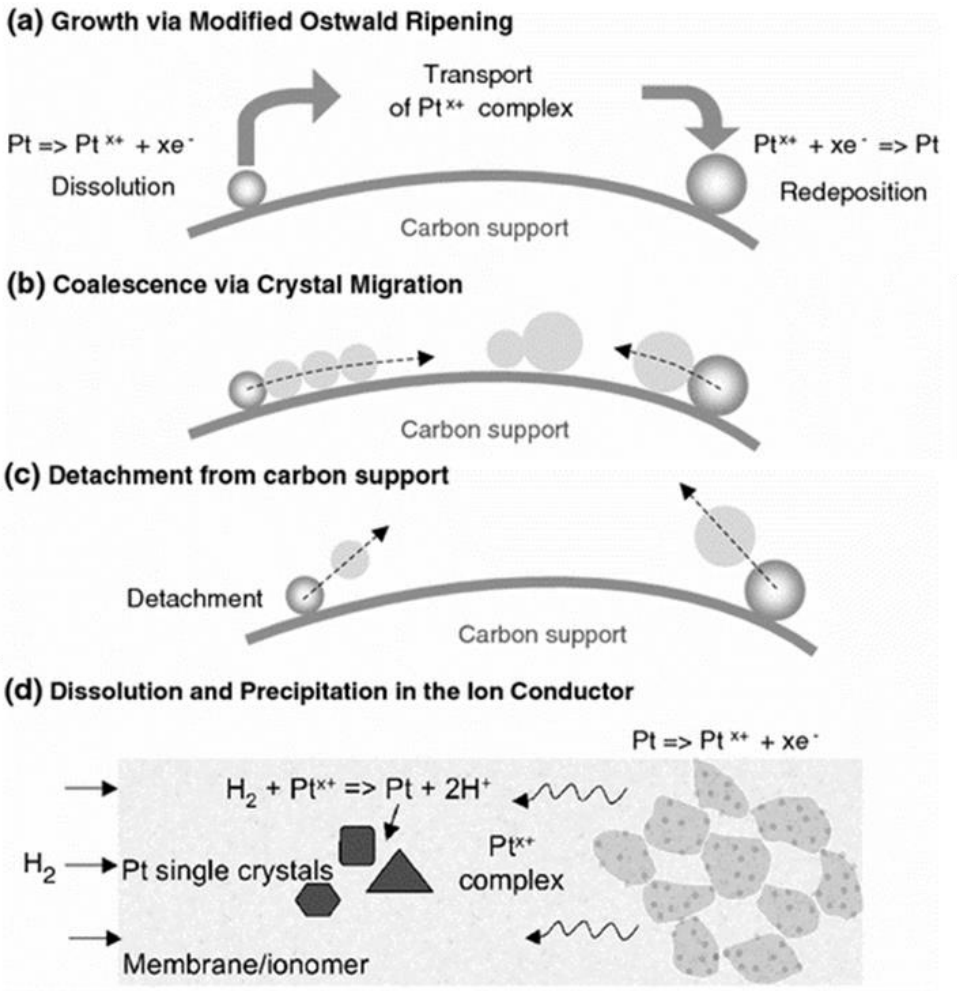


*Figure 2 Four mechanisms for the degradation of supported Pt nanoparticles: (a) Ostwald ripening, (b) coalescence or agglomeration, (c) detachment and (d) dissolution. Adapted with permission, Y. Shao-Horn et. al., Top. Catal., 2007, 46, 285–305. Copyright 2007, Springer Nature.*

Ostwald Ripening

Ostwald ripening is a term ascribed to the behaviour of small particles, which are thermodynamically unstable and thus favour aggregation, in order to lower their surface energy, unless a means is found to prevent this *i.e.* the introduction of a protective capping layer. Surface atoms of small NPs may dissolve into the electrolyte, re-depositing onto surfaces of larger NPs, leading to the formation of much larger NPs and a subsequent reduction of the surface free energy of the particles, which is the driving force of this process.[46] As a result of this, there is a net surface area loss of the Pt NPs, which may reduce their efficiency towards catalysis.[45]

Agglomeration

As with Ostwald ripening, the unprotected Pt NPs show strong preference for agglomeration into larger structures in order to reduce their surface free energy. Rather than dissolving into the electrolyte, agglomeration involves the migration of smaller particles over the electrode surface. The result is a particle size distribution skewed toward larger particles.[47,48]

Detachment and Dissolution

Detachment and dissolution are generally dependent on the electrolyte pH and applied potential, generally taking place at high potentials.[49] Degradation effects are more prominent in particles of diameter below 2 nm, and may also be the result of a weaker interaction between the Pt and supporting electrode.[48] Both mechanisms result in both a larger particle size distribution, and a decrease in electrochemical surface area.[50]

## 2.3 Thiols on Metal Surfaces

Synthesis of nanoparticles often involves the addition of ligands, with examples being alkylphosphine oxides, alkylamines and alkanethiols.[51] These molecules aid in prevention of further nucleation and growth of the particles, and thereby tune the nanoparticle morphology, size and shape.[52] Thiols are commonly employed for this purpose, as they adsorb as self-assembled monolayers (SAMs) on the particle surface, thereby stabilising the metallic core and preventing further growth and aggregation of particles.[53]

Thiol-protected nanoparticles, while stable, are generally less suitable for catalytic applications. This is due to the passivation of their surface, blocking active sites on the nanoparticle surface.[54] It is therefore typically a requirement to remove the thiols from the metal surface *e.g.* reductive desorption of thiols.[55,56]

A study by Williams and Gorman[57] attempted to compare the reductive desorption of alkanethiols from Au and Pt electrode surfaces. Thiol desorption was performed by holding the applied potential at negative potentials for a period of 30 s. The study concluded that SAMs of thiol are easier to remove from Pt versus Au, due to the weaker energetics of the Pt-S bond. [58,59] Observation of a desorption peak is also not seen in voltammetric measurements, due to the slow kinetics of the process.

Furthermore, the thermal stability of SAMs on Au and Pt substrates provides further evidence for the weaker energetics of Pt-thiol bonding as compared to Au-thiol. A study by Vericat *et. al.* demonstrated that thiol SAMs on an Au (111) surface desorb beyond a temperature of 400 K, with the thiolates that remain on the surface going on to adopt a "lying-down" configuration.[55] These remaining thiolates are desorbed as the temperature is raised further, beyond 500 K. In comparison, thermal desorption on a Pt (111) surface takes place at approximately 300 K. A final conclusion from this investigation was the lack of evidence toward any restructuring of Pt upon thiol removal.

Given these insights into the energetics of Au and Pt interactions with thiols, it was expected that the removal of the ligand shell would be easier from the Pt particles than the Au.

## 2.4 Synthesis of Nanoparticles

In order to achieve small sizes of between 1 and 4 nm, synthetic methods to produce nanoparticles must be chosen carefully. Generally, the approaches may be classified as 'wet' or 'dry' synthesis.[60] Examples of each of these methods are explored in this sub-section.

### 2.4.1 Dry Synthesis

Synthesis of nanoparticles in the gas phase is a dry method, with many approaches having been explored and reported in detail.[61] One such method is the use of furnace flow reactors, in which the source material, *e.g.* Ag, is placed in a source such as an oven or a tubular furnace under the flow of an inert carrier gas. The system is heated to temperatures between 350 °C and 1700 °C,[62] with the temperature of the furnace having a significant effect on the morphology of the nanoparticles, and particularly in bimetallic alloy systems.[63] As heat is applied, the target material is vaporised and transferred to cooler areas of the system via the carrier gas stream, where the nanoparticles are formed via cooling and subsequent condensation. Other approaches include the use of pulsed lasers, electrospray systems, and homogeneous nucleation within aerosol droplets.[61] Limitations of these methods include the fast particle formation kinetics often resulting in agglomeration of the nanoparticles.[64] Further, the nanoparticles often need the addition of a protecting layer due to their high sensitivity toward gas molecules, though present in trace amounts.[60]

### 2.4.2 Wet Synthesis

Colloidal methods are an example of a wet synthetic method and allow excellent control over particle morphology and size distribution.[64] There are generally two well-known routes: 'top-down' and 'bottom-up'. Examples of top-down routes include etching of sub-nanometre sized particles from clusters of the target material, ligand exchange and ligand-induced etching processes.[2,16] More commonly employed, 'bottom-up' processes include the Brust-Schiffrin method and electrochemical synthesis, which will be the focus of discussion.

<u>Brust-Schiffrin</u>

A common 'bottom-up' method is the reduction of a metal precursor salt to produce its nanoparticles, an example being the one-phase water-and-citrate-based reduction of a metal salt to produce its nanoparticle suspension, as reported by Turkevich *et. al.*[65] The reducing agent used in these processes, as well as the precursor salt and reactant conditions, play a

role in the resultant nanoparticle core size and morphology.[2] Brust *et. al.* developed a two-phase synthesis for preparation of Au NPs, in which chloroauric acid ($AuCl_4^-$) is transferred from an aqueous phase to an organic phase in toluene, via a phase-transfer reagent of tetraoctylammonium bromide (TOABr). The salt is then reduced via addition of sodium borohydride ($NaBH_4$) in the process of a thiol, which provides stabilisation of the nanoparticles at the desired size.[66] A schematic of this process is presented in Figure 3 (adapted from Qian *et. al.*[40]).

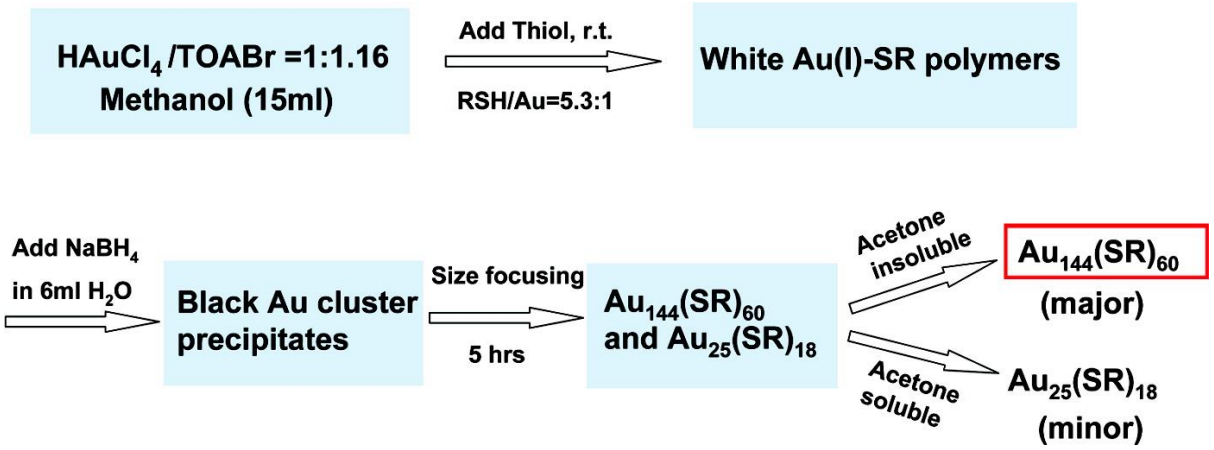


*Figure 3 Schematic of the synthetic method for the preparation of Au clusters. Adapted with permission, H. Qian and R. Jin, Chem. Mater., 2011, 23, 2209–2217. Copyright 2011 American Chemical Society.*

Both the thiol and the reducing agent, when adsorbed onto the surface of growing nanoparticles, aid in the prevention of Ostwald ripening via electrostatic repulsion. An important feature in the synthesis of MNPs is their physical isolation, preventing aggregation in the bulk solution.[67] As such, the importance of the reducing agent and its influence on the nanoparticle size can be derived, as higher concentrations, within limits, provide more rapid coverage and stabilisation of growth of nanoparticles, allowing for size tuning.[46]

These methods are not without their drawbacks, including the potential for loss of precious metal between reaction steps, and the use of often toxic precursor salts *e.g.* hexachloroplatinate ($H_2PtCl_6 \cdot xH_2O$). A further critical aspect can be the cleaning of the final nanoparticle suspensions, as full and ensured removal of both reacting agents and excess thiol species can be a difficult and time-consuming process. As a result, a well-established protocol should be in place for the purification of the nanoparticle samples, as a failure to ensure this

may affect their effectivity *e.g.* in catalysis. These limitations affect the scalability of the methods but provide the control of particle morphology necessary for system optimisation.

Cathodic Corrosion

Another 'wet' synthetic method, cathodic corrosion is an approach in which a bulk metal electrode is converted into an aqueous suspension of its nanoparticles. This approach also allows for good control over properties such as particle morphology and composition.[68] The NPs produced can further be tuned by varying the synthetic parameters, *e.g.* frequency of the square waveform applied to the electrode.[69] Advantages of this approach include the reduction of costs in starting materials, setup and loss of material during reaction steps versus previous methods. Generally, the procedure may continue for a time after the initial setup without continuous observation. The typical set-up for the procedure is shown in Figure 4 (adapted from Rodriguez *et. al* [68]).

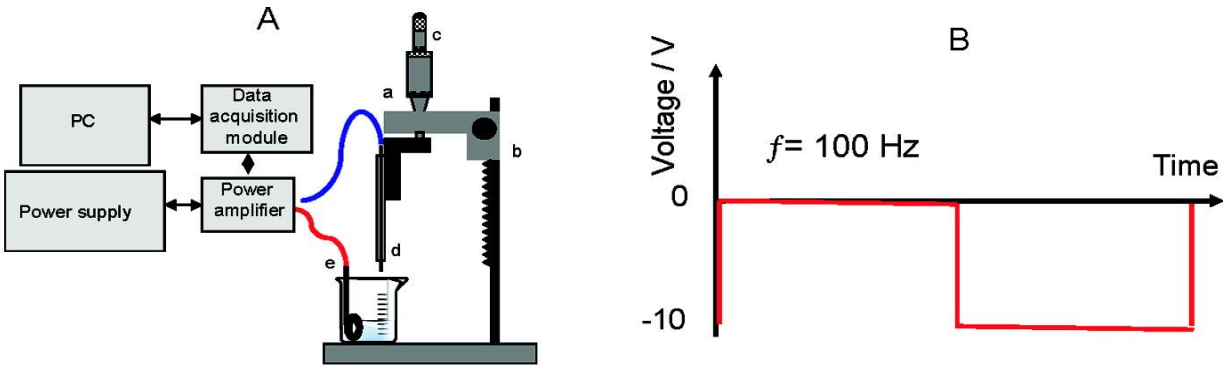


*Figure 4 (A) A diagram for the experimental setup for the cathodic corrosion synthesis of nanoparticles, with features: (a) support, (b) coarse screw, (c) fine micrometric screw, (d) working electrode, and (e) high surface area electrode. (B) The AC waveform applied to the Pt wire working electrode (WE) for preparation of nanoparticles. Adapted with permission, Rodriguez et. al., J. Am. Chem. Soc., 2011, 133, 17626–17629. Copyright 2011 American Chemical Society.*

A micrometric screw is used to lower the working electrode (a wire of the material of interest *e.g.* Pt, Pd, *etc.*) into the solution, in which there is also a high surface area counter-electrode. A power supplier and amplifier allow control of applied potential and frequency. An offset may be applied to the square wave, and is the potential by which the waveform is offset from zero, to allow for the metal wire to remain cathodic throughout the AC cycle (shown in Figure 4 B) and therefore give a faster decomposition into NPs.[70]

The metal wire was lowered into the solution at a set length (typically 2 mm) and allowed to complete a cathodic corrosion cycle-the point at which the current output reaches zero, indicating the decomposition of the immersed wire-before more wire was added. It should be noted, however, that a current output may stabilise at, or slightly above, a value of zero due to passivation of the working electrode (WE), in cases where nanoparticles do not disperse upon formation. A plot of the maximum current measured during the half-cycles is shown as a function of time in Figure 5, for the synthesis of Pt NPs in alkaline media. The current recorded decreases as a function of time, as the submerged section of the metal wire begins to decompose under the applied AC bias.

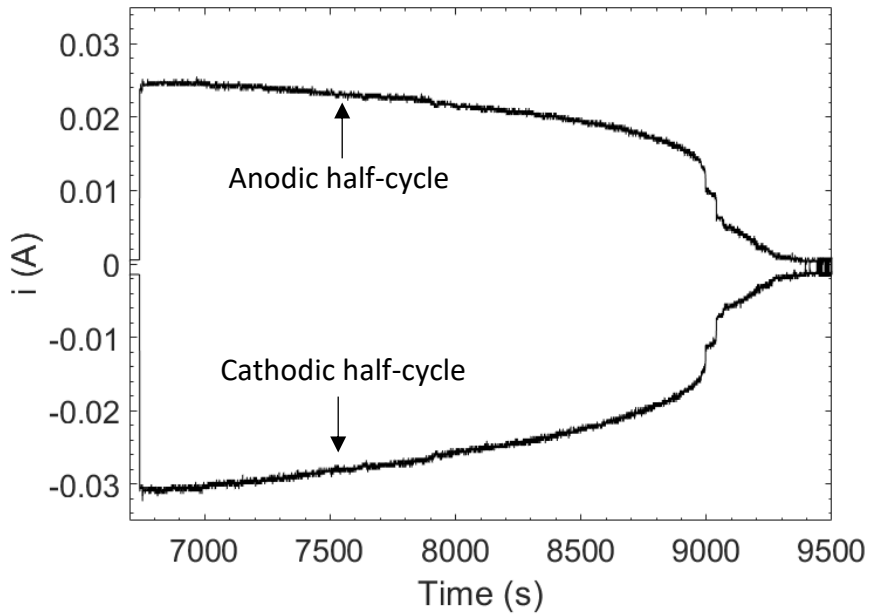


*Figure 5 A current versus time plot for the preparation of Pt NPs in this project, measured in 0.1 M NaOH (Freq. 100 Hz, Amplitude 1.25 V, Offset -1.25 V). The Pt wire diameter was 0.05 mm and was immersed 2 mm into the electrolyte, with a Pt flag as reference electrode*

In this work, Pt NPs were synthesised using the cathodic corrosion method in alkaline media (0.5 M NaOH). The applied parameters were a frequency of 100 Hz, duty cycle 50%, amplitude of 1.25 V and an offset of -1.25 V. The successful production of nanoparticles is dependent on parameter settings, as the electrolyte (molarity) and corrosion parameters (*e.g.* potential window) determine whether the wire undergoes corrosion, and how rapid that process is. A model for the cathodic corrosion of a Pt wire in alkaline media has been presented by Yanson *et. al*, in which two possible routes are discussed.[71]

The primary stage is the same for both routes, in which the reduction of water in the electrolyte leads to a great amount of hydrogen gas evolution. As such, a layer of high pH is formed at the surface of the wire *i.e.* the cathode. This layer is rich in alkali cations ($Na^+$) and contains only enough water to stop the reduction of these cations and keep the layer in a liquid state.

The first route suggests that under cathodic potentials, the surface of the Pt wire is reduced into its anions, which are stabilised by the surrounding alkali cations, forming a complex. This complex is then solvated in the cation-water layer and diffuses away from the wire. The Pt anions are then oxidised upon entering the free water, producing $H_2$ and becoming charge neutral Pt atoms which then agglomerate to form nanoparticles.

An alternative approach is that the Pt wire, under cathodic polarisation conditions, transfers its electrons to the protons in water. This step must take place through the cation layer surrounding the electrode. Pt anions thereby act as electron transfer agents, becoming charged at the surface of the wire and moving through the cation layer, stabilised through the diffusion by the $Na^+$ cations. The anions then discharge when they enter the free water, and as previously, agglomerate into nanoparticles.[71]

The presented models also explain the effect of electrolyte concentration on the dispersion of nanoparticles. If the electrolyte is not sufficiently concentrated, the cation-water layer surrounding the electrode is not sufficiently thick to allow the anions to diffuse away from the wire. These then agglomerate and passivate the wire, eventually inhibiting further synthesis. This is also a reason for the AC voltage being used, as it aids in the detachment and dispersion of nanoparticles.[72]

## 2.5 Physical Characterisation Techniques

### 2.5.1 UV-Vis Spectroscopy

Noble metal nanoparticles on the nanoscale exhibit unique electronic and optical properties, for example surface plasmon resonance (SPR). SPR is a phenomenon observed in metallic nanoparticles of a certain size, where their interaction with light causes the collective oscillation of the free electrons in the metal.[73]

It has been shown that Au clusters with a diameter greater than 10 nm give a UV-Vis spectrum with a large SPR peak, with some variation in the wavelength at which it is observed- typically

in the range of 500 and 600 nm.[74,75] The presence or absence of this feature in the UV-Vis spectra of a nanoparticle sample can be a good early indicator of the particle size.

### 2.5.2 Transmission Electron Microscopy (TEM)

TEM is a microscopy technique that exploits the small wavelengths of electrons, which are transmitted through a sample in order to produce images that allow for quantitative size distribution analysis of nanoparticle samples.[76] Generally, electrons are accelerated via an electromagnetic field and travel from the source through a vacuum, after which they pass through the sample. For good resolution, the samples must be sufficiently electron-transparent to allow electrons to pass through, typically below 90 nm.[77] This also aids in minimisation of electron scattering, which decreases the number of electrons to be detected and therefore can affect the accuracy of the image obtained. The electron transmission and diffraction data are then processed by the system, resulting in a two-dimensional image. An example can be seen in Figure 6, which presents Au nanoparticles imaged as part of this project.

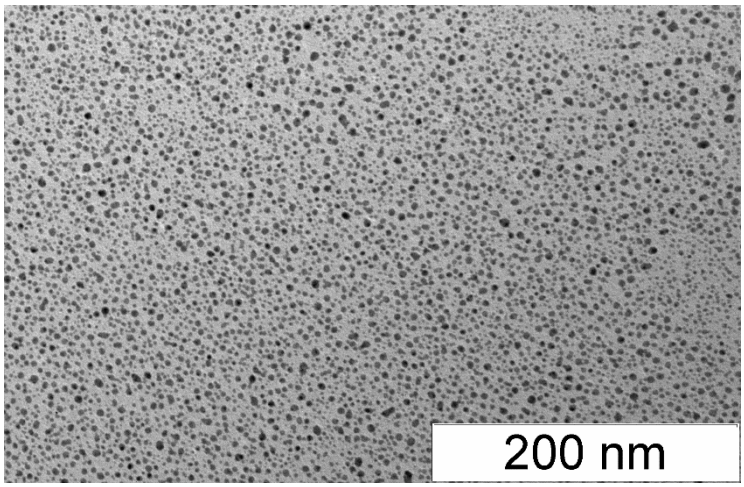


*Figure 6 A TEM image of $Au_{144}(HT)_{60}$ nanoparticles on a copper-carbon grid, taken as part of this project.*

## 2.6 Electrochemical Characterisation

Electrochemical characterisation was preformed after the initial physical characterisation, to give a more in-depth insight toward the properties of the MNPs. Electrochemical experiments involve measurement of one of four parameters: current, time, charge and potential.

### 2.6.1 Cyclic Voltammetry

Cyclic voltammetry is a widely employed electrochemical technique that shows sensitivity towards size and structure, making it a good method for characterisation of electrode surfaces.[78] During cyclic voltammetry measurements, current is measured in response to an overall linear potential-time excitation of the working electrode under investigation. Potential is applied between a selected upper and lower limit and swept between these values at a rate *e.g.* 100 mV $s^{-1}$. One complete 'cycle' consists of a sweep in both the positive (anodic) and negative (cathodic) directions.[79]

A three-electrode electrochemical cell consists of a working electrode (WE), a counter electrode (CE) and a reference electrode (RE). While the WE potential is set relative to the RE, the potentiostat aims to control this potential to the pre-set value, by passing an appropriate current between the WE and the CE. The measured response produces a cyclic voltammogram (CV) plot of current versus potential. Prominent features are peaks in the positive and negative scan directions, which correspond to oxidation and reduction at the electrode surface, respectively.[80]

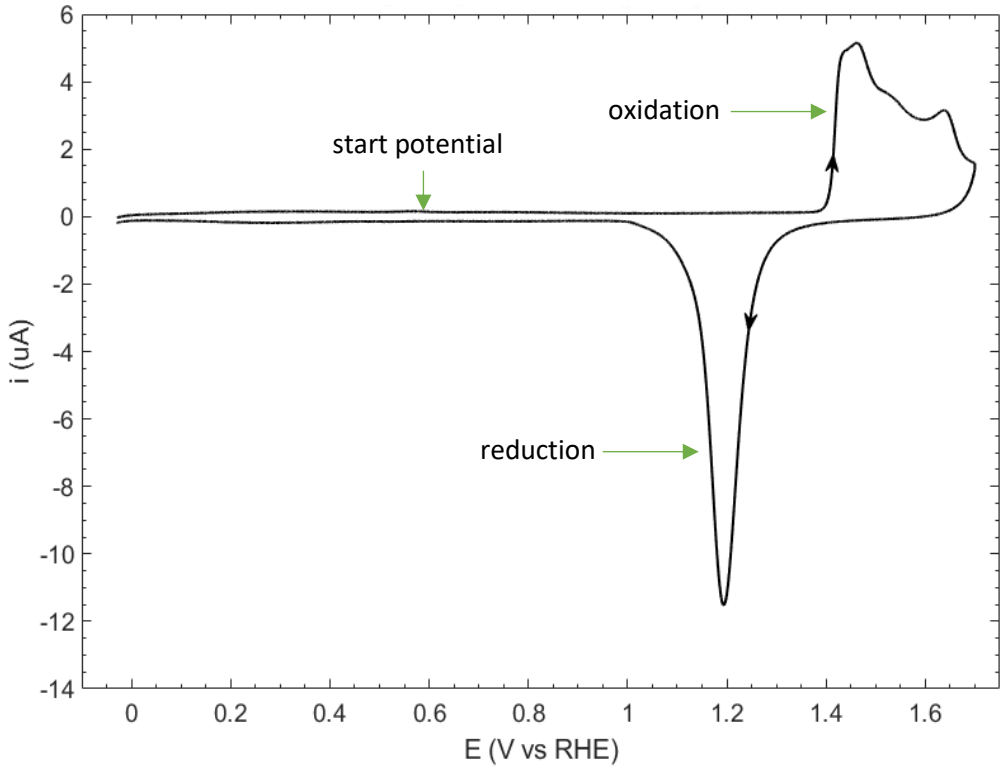


*Figure 7 Voltammetric profile of an Au electrode in 0.5 M $H_2SO_4$, with features **(a)** oxidation peak **(b)** reduction peak. v =0.05 V/s, **CE** = Au, **RE** = SCE (sat'd KCl). Measured values were converted to RHE scale.*

A blank voltammogram is one recorded in a reactant-free environment, and therefore gives information on the cleanliness of the cell and its components (*i.e.* electrolyte and glassware cleanliness), the electrode-electrolyte interface and the electrode surface. The latter is assessed through comparison of the blank voltammograms with known characteristic features in CV profiles. An example of a blank voltammogram can be seen in Figure 7. The CV profile is typical of a polycrystalline gold electrode in sulfuric acid (0.5 M). Recorded with a saturated calomel electrode (SCE) as a reference electrode, the values measured were converted to the reversible hydrogen electrode (RHE) scale for easy comparison between figures. It is to be noted that though the characteristic peaks for gold activity are generally the same across literature, there are variations in CV profiles. These can be due to differences in electrode preparation, polishing and cleaning procedures, surface reconstruction during experiments, etc.[79]

The CV parameters are characterised as the initial (starting) potential $E_i$ (0.6 V), an upper and lower vertex potential $E_1$ (1.7 V) and $E_2$ (-0.05 V), while the final potential $E_f = E_i$. The potential sweep rate $v$ at which the measurements are performed is defined as the potential step $D_E$ divided by the time step $D_t$ and is thus in units of V/s.

The CV region below +1.2 $V_{RHE}$ is referred to as the double layer where electrolyte cations in NaOH may adsorb on the Au surface. As the potential increases, the Au surface becomes more positively charged, and electrolyte cations begin to be displaced by OH anions. There is a peak in the positive direction with an onset of 1.37 $V_{RHE}$, which corresponds to the formation of an Au-O layer, referred to as oxide formation.[79] There are minor features present after this, though no major changes are observed until the potential window moves upwards into the oxygen evolution region (not shown in the accompanying figure). The surface oxides formed are reduced in the negative scan, as the potential becomes more negative again, and as such we have a reduction peak.

# 3. Experimental

## 3.1 Glassware Cleaning Procedures

### 3.1.1 Nanoparticle Synthesis

All glassware was cleaned prior to use via immersion in boiled $HNO_3$/water (1:3 ratio) and rinsed thoroughly with water before drying in an oven overnight at 70 °C.

### 3.1.2 Electrochemistry

All glassware was cleaned before experimental work to ensure reproducible experimental conditions. The glassware was immersed overnight in a solution of acidic permanganate ($KMnO_4$). Upon removal from the $KMnO_4$, the glassware was rinsed firstly with water (Elga, resistivity >18.2 MΩ cm, 1 ppb total organic content), and then with a diluted solution of $H_2SO_4/H_2O_2$ (a 1:3 ratio). Finally, the glassware was rinsed with boiling water at least 4 times.

## 3.2 Au NP Synthesis

The reagents used for the synthesis were gold (III) chloride trihydrate ($HAuCl_4 \cdot 3H_2O$, Sigma Aldrich ≥99.9%), tetraoctylammonium bromide (ToABr, Sigma Aldrich, ≥99%), methanol (Sigma Aldrich, 99.9%), 1-hexanethiol (HT, Sigma Aldrich 95%), dichloromethane (DCM, Sigma Aldrich, ≥99.9%) and acetone (VWR, 99%). Ultrapure water used throughout experimental work (Elga, resistivity >18.2 MΩ cm, 1ppb total organic content).

The synthesis followed previously reported procedures.[40] $HAuCL_4$ (236 mg) and ToABr (380 mg) were dissolved in methanol (30 mL), and the solution stirred vigorously for 15 min. At this stage, 1-hexane-thiol (0.476 mL) was added, and stirring continued for another 15 min. A freshly prepared solution of $NaBH_4$ (0.5 M, 6mL) was added under fast stirring, and the mixture became black due to the reduction of the Au salt into Au NPs. The mixture was covered and allowed to stir overnight (~14 hrs), after which the mixture was dried under vacuum filtration.

The sample was washed ten times with an excess of methanol, to ensure the removal of excess thiol. DCM was added to separate the Au NPs from Au(I)-SR polymers, as the latter show very poor solubility in DCM.

Acetone was then used to separate smaller $Au_{25}(HT)_{18}$ clusters from $Au_{144}(HT)_{60}$ (HT: 1-hexanethiol), as the $Au_{25}$ nanoparticles are soluble in acetone while the latter are not. Finally,

the $Au_{144}$ nanoparticles were re-dissolved in DCM, and the Au samples kept in sealed glass vials.

### 3.2.1 Characterisation

UV-Vis Spectroscopy

The Au NPs were characterised initially using UV-Vis spectroscopy. Measurements were performed using a UV-Vis spectrophotometer (Aligent Technologies, Cary 60 UV-Vis) and curvettes (Fisherbrand, polystyrene).

TEM Imaging

TEM measurements were performed using a JEOL-1400 Bio-TEM instrument. The Au NP solution was sonicated in a water bath, before being drop cast onto carbon-copper grids (carbon film on 300 mesh copper, EM Resolutions) and allowed to air dry.

## 3.3 Pt NP Synthesis

Brust-Schiffrin Synthesis

The synthesis was carried out via platinum salt reduction. Solutions were prepared from ToABr (Sigma Aldrich, ≥99%), toluene (Sigma Aldrich, 99.8%), dihydrogen hexachloroplatinate ($H_2PtCl_6 \cdot xH_2O$, Alfa Aesar, 99.999%) and sodium borohydride ($NaBH_4$, Sigma Aldrich, ≥98%). Water used throughout experimental work was ultrapure (Elga, resistivity >18.2 MΩ cm, 1ppb total organic content).

A solution of the phase transfer reagent ToABr (1.1 g) and toluene (40 mL) was added to a solution of the Pt salt, $H_2PtCl_6 \cdot H_2O$ (0.1857 g) in 15 mL water. This mixture was stirred using a magnetic stirrer, until all the Pt has transferred into the organic phase. This was indicated by a colour change from yellow to colourless in the aqueous phase, a result of the absence of Pt. The organic phase was then separated, and a freshly prepared solution of $NaBH_4$ (0.19 g) added under vigorous stirring. After 2-3 minutes, a colour change was observed from orange to brown, and the two-phase system was allowed to stir for a further 30 mins. The organic phase was separated and washed in three stages: once with $H_2SO_4$, twice with $K_2CO_3$, and five times with water. The final solution was dried over $MgSO_4$ and the toluene evaporated using a rotary evaporator.

Cathodic Corrosion

A platinum wire (Alfa Aesar, 99.95%) was used as the cathode for the production of Pt NPs via cathodic corrosion. The wire was lowered into vessel containing 20 mL of 0.5 M NaOH (VWR, ≥ 98.5%) electrolyte, and a high surface area Pt flag as a counter electrode. An image of the reaction vessel is included below in Figure 8.

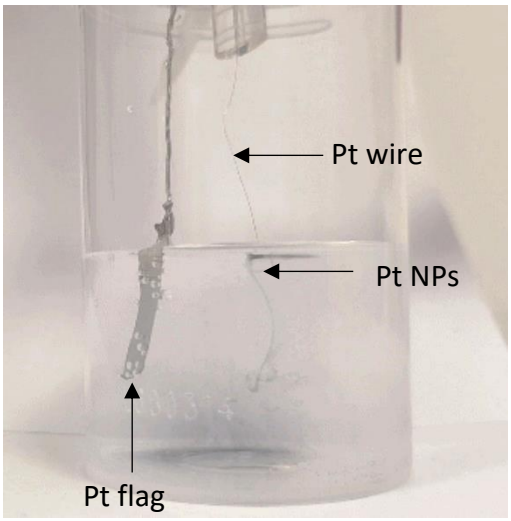


*Figure 8 Setup of the production of Pt NPs using a Pt wire (WE) and large surface area Pt flag (CE), in 0.5 M NaOH electrolyte.*

An AC square wave form was applied between 0 and -2.5 V (amplitude ±1.25 V, offset -1.25 V) under stationary conditions *i.e.* non-rotating. The Pt wire was immersed 2 mm at a time, with 8 mm used in total.

After synthesis, the Pt NP suspension was sonicated, divided into four glass tubes and then placed in a centrifuge for 25 mins, at 3000 RPM. Subsequently, the supernatant was removed and replaced with water. This process was repeated until the supernatant's pH was 11, when 1-hexanethiol (2.5 µL, molar ratio) was added. The sample was then sonicated for 10 mins in order to disperse the thiol throughout the solution. The cleaning procedure was then resumed until a neutral pH was achieved. Finally, a further five washes were conducted to remove excess thiol.

## 3.4 Electrochemistry

For all electrochemical measurements, a three-electrode electrochemical cell was employed with an electrolyte of 0.1 M NaOH (VWR, ≥ 98.5%). Prior to measurements, argon gas was passed through the cell to deoxygenate the electrolyte. A gold flag was used as the CE, and a

SCE (sat. KCl) was the RE. All results were converted to the standard RHE scale for ease of comparison. Measurements were performed using a μAutolab (III) potentiostat. Prior to experiments, the Au and Pt disc micro-electrodes (WE, φ 0.025 mm) were cleaned via polishing with diamond slurry and rinsed thoroughly with water.

# 4. Results and Discussion

## 4.1 Au NP Synthesis

### 4.1.1 UV-Vis Spectroscopy

UV-Vis spectroscopy allowed for an initial determination that the nanoparticles were below 10 nm in size due to the absence of a SPR band in the spectrum. The resultant UV-Vis spectrum is presented in Figure 9. Comparison with results from Pensa *et. al* [6] (inset) also gave some insight into the success of the synthesis.

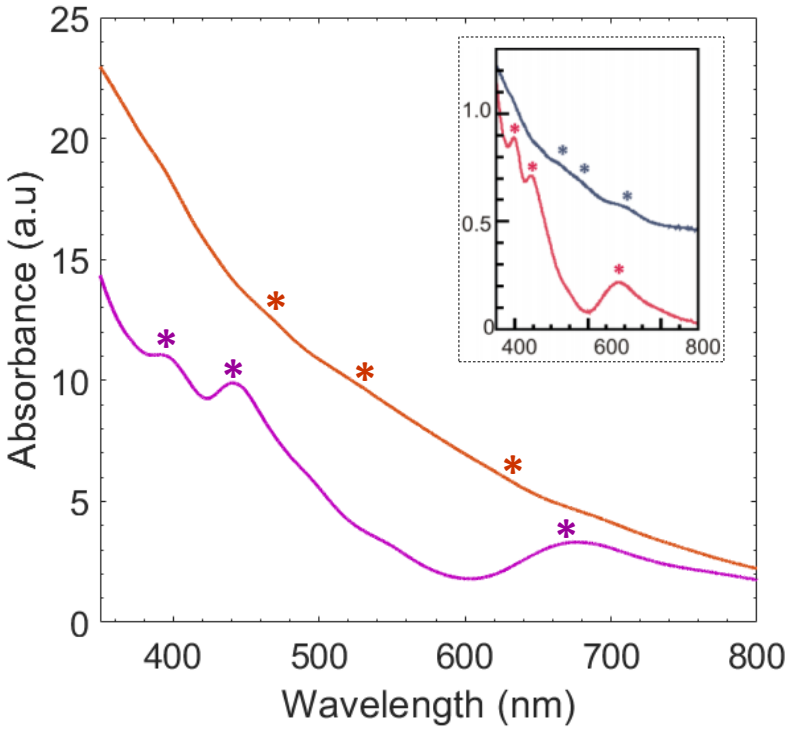


*Figure 9 UV-Vis spectra of Au NP samples; $Au_{144}(HT)_{60}$ (orange), $Au25(HT)_{18}$ (purple). Au characteristic peaks are highlighted using markers.* ***Inset:*** *UV-Vis spectra of Au NP samples by Pensa and Albrecht. Inset adapted with permission, E. Pensa and T. Albrecht, J. Phys. Chem. Lett., 2018, 9, 57–62. Copyright 2018 American Chemical Society.*

Absence of the SPR band was a good first indication that the nanoparticles were successfully below 3 nm in size, as was the aim and expectation during synthesis. Characteristic absorption bands observed are listed in Table 1.

| Sample | Wavelength (nm) | | |
|---|---|---|---|
| **$Au_{144}$** | 470 | 520 | 680 |
| **$Au_{25}$** | 390 | 440 | 680 |

*Table 1 From experimental data, position of absorption bands for two cluster sizes of gold nanoparticles; $Au_{144}(HT)_{60}$ and $Au_{25}(HT)_{18}$. Approximate concentrations were calculated as: $[Au_{144}(HT)_{60}] = 1.53\ mg\ mL^{-1}$, $[Au_{25}(HT)_{18}] = 7.12\ mg\ mL^{-1}$*

Though UV-Vis spectroscopy provided useful initial information, further insight was needed with respect to the particle size and distribution. It is important to note at this stage that as the particles of interest were the $Au_{144}(HT)_{60}$, the term Au NPs will be used only to reference the samples of this composition in further discussion of results.

### 4.1.2 TEM Imaging

A TEM image of the Au NPs, and the subsequent size distribution data (Gaussian fit), is shown in Figure 10. The average particle size was computed using ImageJ software, and was found to be 2.8 ± 0.1 nm. This is in line with expectations from the synthetic method.

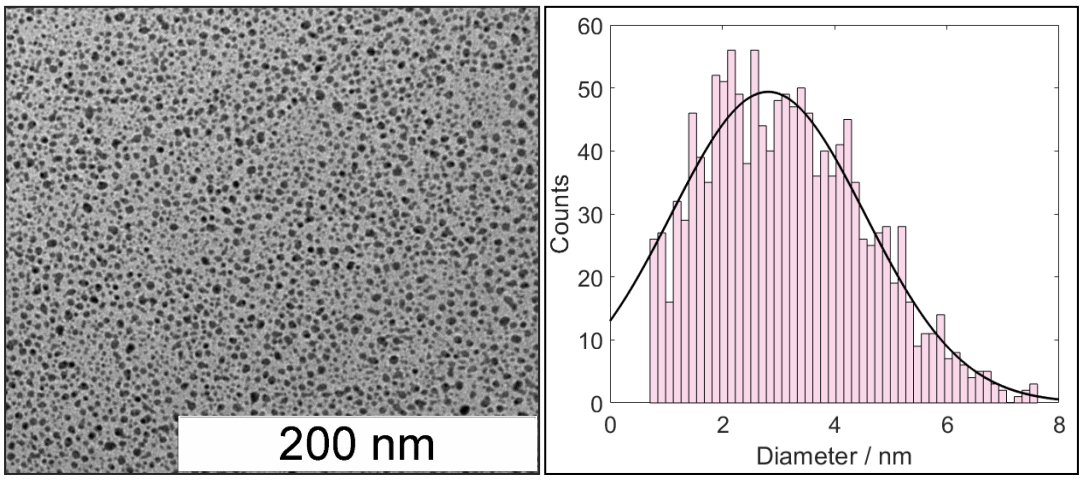


*Figure 10 TEM image and particle size distribution of Au nanoparticles. Imaging was done using a JEOL-1400 Bio-TEM, with assistance of Dr Anton Vladyka.*

## 4.2 Pt NP Synthesis

### 4.2.1 Synthetic Procedure

The Brust-Schiffrin synthetic protocol provided some issues, namely the evaporation of toluene in the final step. It was attempted several times but proved unsuccessful. As a result, the cathodic corrosion method was instead explored. The latter method provided a relatively quick turnover of synthesis, with the nanoparticles produced being easy to clean and

implement in experimental work. For this reason, cathodic corrosion was used for Pt NP synthesis for the remainder of the project.

### 4.2.2 TEM Imaging

Analysis of TEM images for the samples were difficult, due to poor resolution. An example of an image taken is shown in Figure 11. Some beam damage of the sample may have occurred, as the sample appeared to move when the electron beam focus was increased. Manual analysis of 50 nanoparticles gave an average particle size of 3.1 ± 0.5 nm.

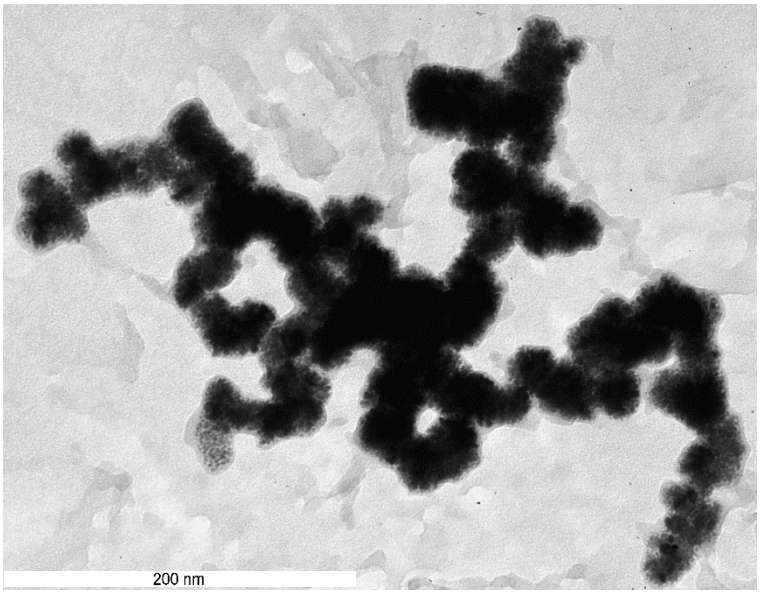


*Figure 11 TEM image of Pt nanoparticles. Imaging was done using a JEOL-1400 Bio-TEM, with assistance of Dr Anton Vladyka.*

## 5. Electrochemistry of Au and Pt NPs in 0.1 M NaOH

After synthesis and initial physical characterisation, electrochemical experiments were employed to evaluate the thiol-redistribution from nanoparticles onto the bulk metal electrode surface. Leading on from previous work involving an Au surface/AuNP system, the combinations used in this project were Au surface/PtNP and Pt surface/AuNP. As Au and Pt have different characteristic response features within their voltammetric profiles, the emergence of new-or indeed influence over existing- characteristic features would indicate the nanoparticles were exposed and therefore catalytically active, due to the re-distribution of the ligand shell.

The electrode surfaces were modified via immersion into the respective nanoparticle samples for 24 hours, to allow ample time for surface coverage of the electrodes. Preceding this, blank voltammograms were recorded of the Au and Pt micro-electrodes, allowing for comparisons between the electrode surfaces after surface modification.

### 5.1 Au Electrode Surface

A CV recorded for the Au micro-electrode in 0.1 M NaOH (pH 13) is shown in Figure 12. The voltammogram profile is in general agreement with the reported behaviour of bulk Au

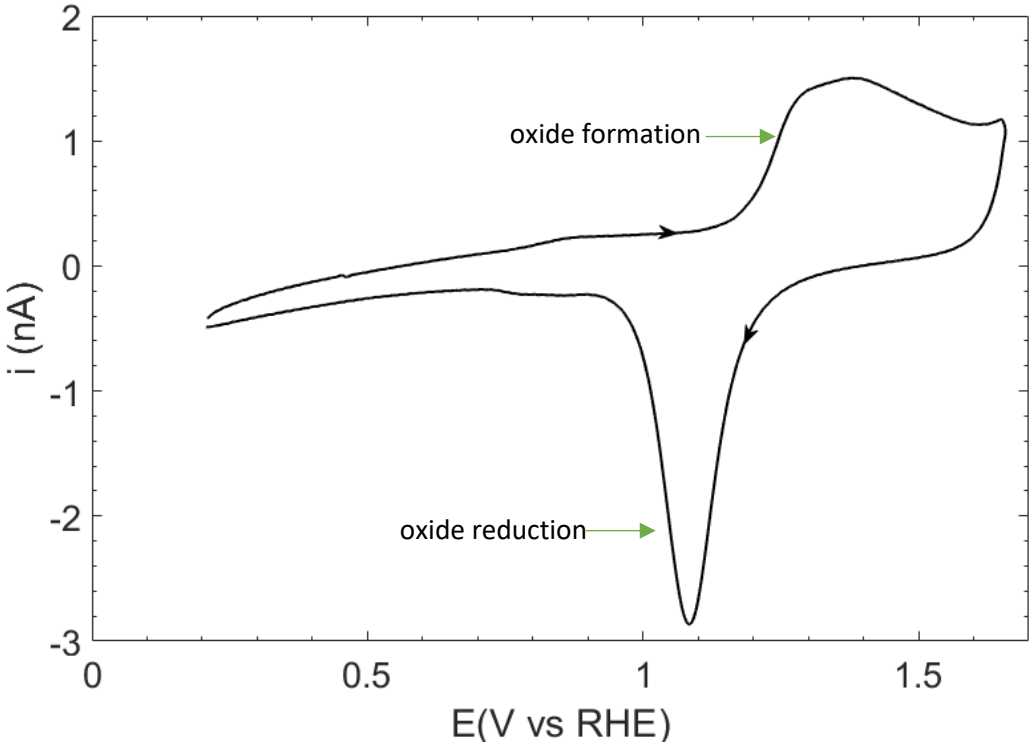


*Figure 12 The blank voltammetric profile of an Au electrode in 0.1 M NaOH. v= 0.05 V/s*

in literature.[81]

## 5.2 Pt Electrode Surface

The blank voltammogram of the Pt electrode is shown in Figure 13. For ease, the CV may be split into three regions: the hydrogen region, the double-layer region and the oxide region.[82]

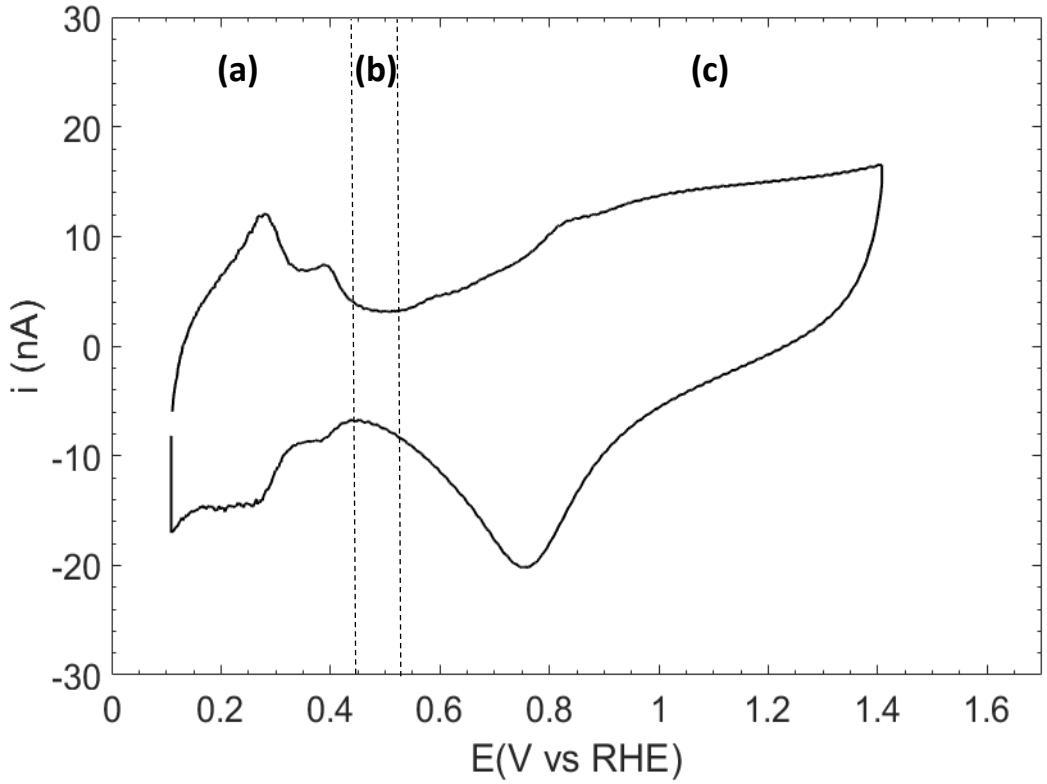


*Figure 13 The blank voltammetric profile of a Pt micro-electrode in 0.1 M NaOH. The CV has been divided into **(a)** hydrogen **(b)** double layer and **(c)** oxygen region. v = 0.05 V/s*

Hydrogen Region

In the positive direction, we see peaks with an onset of 0.20 $V_{RHE}$, corresponding to hydrogen desorption at Pt (110) and (100) sites. In the negative sweep, peaks in positions corresponding to those in the positive scan are observed, with onsets of 0.41 $V_{RHE}$ and 0.33 $V_{RHE}$, which are attributed to hydrogen adsorption.[82] In the negative scan, the peak arising at 0.10 $V_{RHE}$ is the beginning of hydrogen gas evolution. The CV presented here was cut off before this region, though it was explored in later measurements.

Oxide Region

As the potential increases in the positive scan direction, a peak is observed at 0.63 $V_{RHE}$, which is attributed to oxide formation at the Pt surface. In the backward direction we see a peak with an onset of 1.0 $V_{RHE}$, which is the reduction of these oxides.[83]

## 5.3 NPs on Au and Pt Electrode Surfaces

### 5.3.1 Au surface/PtNP

The Au electrode surface was modified with PtNPs, giving Au surface/PtNP. The CV of this surface can be seen below in Figure 14. With respect to the characteristic peaks, there is little difference in the voltammetric profile of the modified surface when compared to the blank, however there is some change in the double layer region.

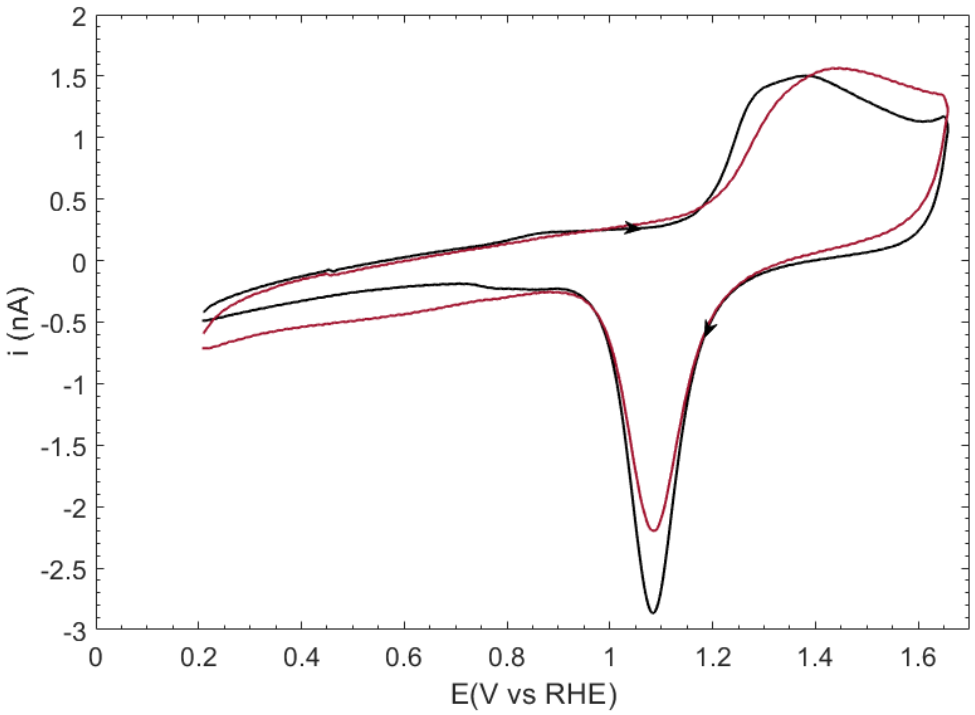


*Figure 14 Voltammetric profile of the bare Au electrode surface (**black**) and Au surface/PtNP (Au micro-electrode immersed in PtNPs for 24 hours) (**red**) in 0.1 M NaOH. v = 0.05 V/s*

It has been shown that the double layer and surface oxidation regions are dependent on electrode surface structure.[78,81] With blank voltammograms of the Au electrode surface being largely reproducible, it could be theorised that influence of some Pt NP on the Au surface could have affected the voltammogram. However, as no Pt activity can be determined from the CV profile, the particles may remain protected on the electrode surface. To further explore this, the potential window was opened negatively to reductively desorb the thiols, in

order to confirm the presence of the Pt nanoparticles on the electrode surface. The resulting voltammogram is presented in Figure 15. To note regarding the bare Pt electrode CV, the peak present at 0.65 $V_{RHE}$ in the positive scan direction is likely due to an impurity.

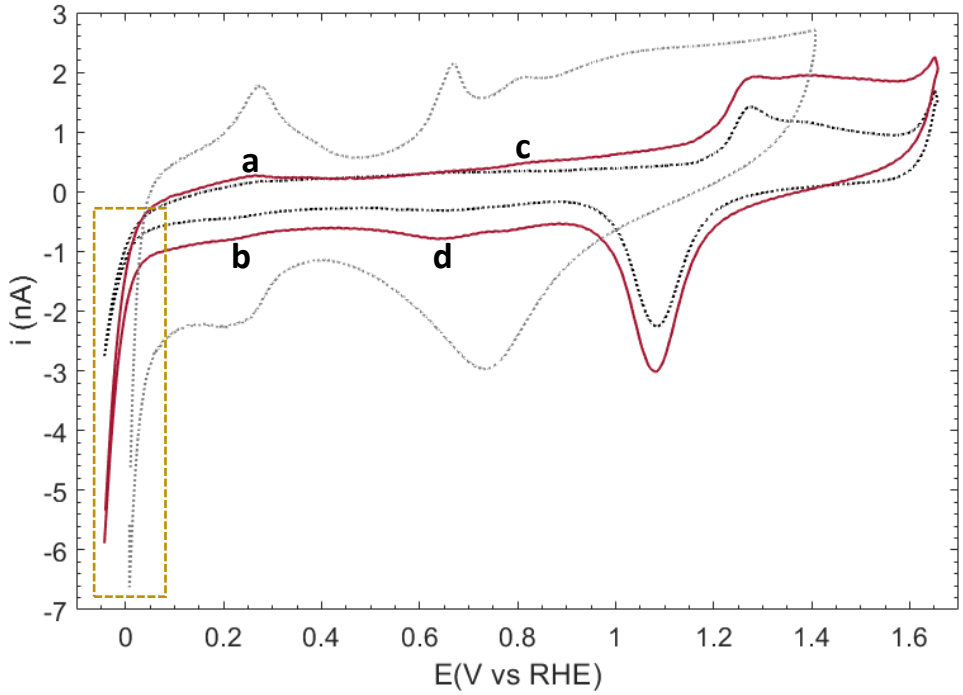


*Figure 15 Voltammetric profiles of the bare Au electrode surface (dotted black), Au surface /PtNP (Au micro-electrode immersed in PtNPs for 24 hours) (**red**), and bare Pt electrode surface (dotted grey) in 0.1 M NaOH. Peaks a,b,c and d correspond to Pt characteristic peak positions. Yellow box indicates the hydrogen gas evolution region. v = 0.05 V/s*

There is a clear difference in the voltammetric profile of the modified surface (red line) as compared to the blank (dotted black) when the potential window is opened. A small peak at 0.82 $V_{RHE}$, observed in the negative scan of both the Au blank and the modified surface, may be attributed to the reduction of a hydrous gold oxide species.

The most noticeable change may be the appearance of peaks (**a→d**) in the otherwise uncharacteristic double layer region. Upon further examination, these peaks seemingly correspond to the positions of characteristic Pt peaks, as observed in Figure 13, which has been overlaid (grey, dotted line) for comparison.

Further, there is a difference in the behaviour of the modified surface in the hydrogen gas evolution region (highlighted by the yellow box). The electrochemical response of the modified surface is more similar in nature to that of the bulk Pt, versus bulk Au, in this region. It can be assumed that the increase in the potential window gives the reduction of the metal-thiol bond, thereby desorbing the thiol and resulting in the emergence of Pt features.

The Pt-thiol bond energy is much weaker than that of the Au-thiol bond, with thiol monolayers on Pt being generally less ordered.[58,59] An enthalpic consideration therefore suggests that the thiols would favour a redistribution onto the gold surface, agreeing with the entropic argument of redistribution onto the much larger gold electrode surface.[6] This could be due to the many binding sites presented by the bulk electrode surface, in comparison to the nanoparticles.[84]

Detection of Pt characteristic peaks in the Au surface/PtNP system would be indicative of successful thiol surface diffusion, leaving the Pt NPs exposed on the Au surface. A conclusion could not be drawn from these voltammetric profiles in alkaline media alone, and therefore further investigation was required, with a more sensitive electrochemical environment.

### 5.3.2 Pt surface/AuNP

As with the Au surface/PtNP system, the potential window was opened negatively to explore the onset of the hydrogen gas evolution region. Unlike the results seen with the Au surface/PtNP system, no change can be seen in the characteristic peaks of the voltammetric profile. The measured current response is, however, lower as compared to the bulk Pt.

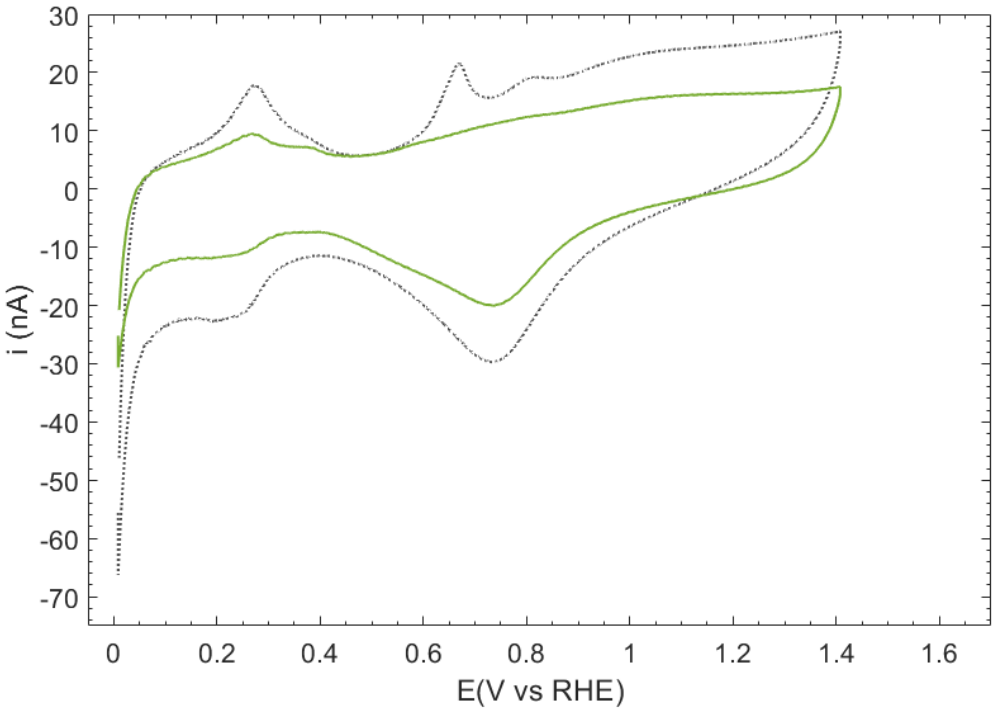


*Figure 16 Voltammetric profiles of the bare Pt electrode surface (dotted grey) and Pt surface /AuNP (Pt micro-electrode immersed in AuNPs for 24 hours) (green) in 0.1 M NaOH. v = 0.05 V/s*

This could be due to the presence of still-protected AuNPs on the electrode surface, blocking some active sites and therefore resulting in a decreased current measured. It could also be the result of the Pt surface becoming potentially contaminated, for example by the remaining thiols.

It is important to note the difference in scale of the current responses recorded for the two bulk metals, with the Pt currents being almost ten times greater than those of Au. It may therefore be the case that any potential AuNP activity is simply masked by the much larger readings of the Pt surface.

## 5.4 Conclusions

Initial electrochemical characterisation in alkaline media indicates that the nanoparticles successfully provide some surface coverage of the metal electrodes, as evidenced by the differences in voltammetric profiles before and after immersion into the Au and Pt nanoparticles.

In the case of these modified electrodes, the emergence of the characteristic features of the respective nanoparticle material (Au/Pt) would indicate the redistribution of the thiol protective layer from the nanoparticle surface onto the bulk electrode surface. From this it could be concluded that the interaction of the nanoparticle with the metal electrode surface is effective in aiding the removal of the thiol shell.

For example, the formation of Pt characteristic peaks in the response of the Au surface/PtNP electrode would suggest a thiol redistribution into the bulk of the Au electrode, resulting in unprotected Pt nanoparticles on the surface being electrochemically active.

The emergence of these Pt features is seen upon thiol-desorption via extension of the potential window. No such effect is seen for the Pt surface/AuNP electrode, potentially due to the 'masking' of any Au electrochemical activity by the much greater intensity of the Pt electrode surface response. Alternatively, the AuNPs may remain protected on the Pt electrode. This would suggest that rather than purely enthalpic or entropic factors driving a redistribution of thiols from the nanoparticles to the electrode surface, there is a combination of the two processes, as has been established in previous work by Pensa *et. al.*[6]

In the cases of both the modified systems (Au surface/PtNP and Pt surface/AuNP), there is an entropic driving force present for the redistribution of thiols from the nanoparticles onto the electrode surface, due to the greater availability of binding sites on the larger electrode surface. As mentioned, the Au-S bond is much stronger versus the Pt-S bond, and so it was predicted that the Au surface/PtNP system would show a greater affinity than the Pt surface/AuNP system toward the redistribution of the thiol shell as a result. Electrochemical responses in alkaline media were insufficient in providing significant conclusions concerning these surface dynamics. The organic compound glycerol was therefore introduced, as the electro-catalytic decomposition of this would provide more distinct and comparable electrochemical responses. These investigations are discussed in the following chapter.

# 6. Electrochemistry of Au and Pt NPs in 0.1 M Glycerol

## 6.1 Introduction

The organic compound glycerol can be oxidised into useful chemicals such as glyceraldehyde and glyceric acid, via its electrocatalytic decomposition.[85] The electro-oxidation of glycerol has been looked at electrochemically in some detail, as redox reactions that dominate the mechanisms of its decomposition, and result in increased sensitivity toward electrochemical measurements. It is important to note, however, that a solely electrochemical approach does not give enough information on the final and intermediate oxidation products. Coupling electrochemical approaches with methods such as Fourier transform infrared (FTIR) and online high-performance liquid chromatography (HPLC) allows further probing into the reaction mechanisms, products, and intermediates.[85,86]

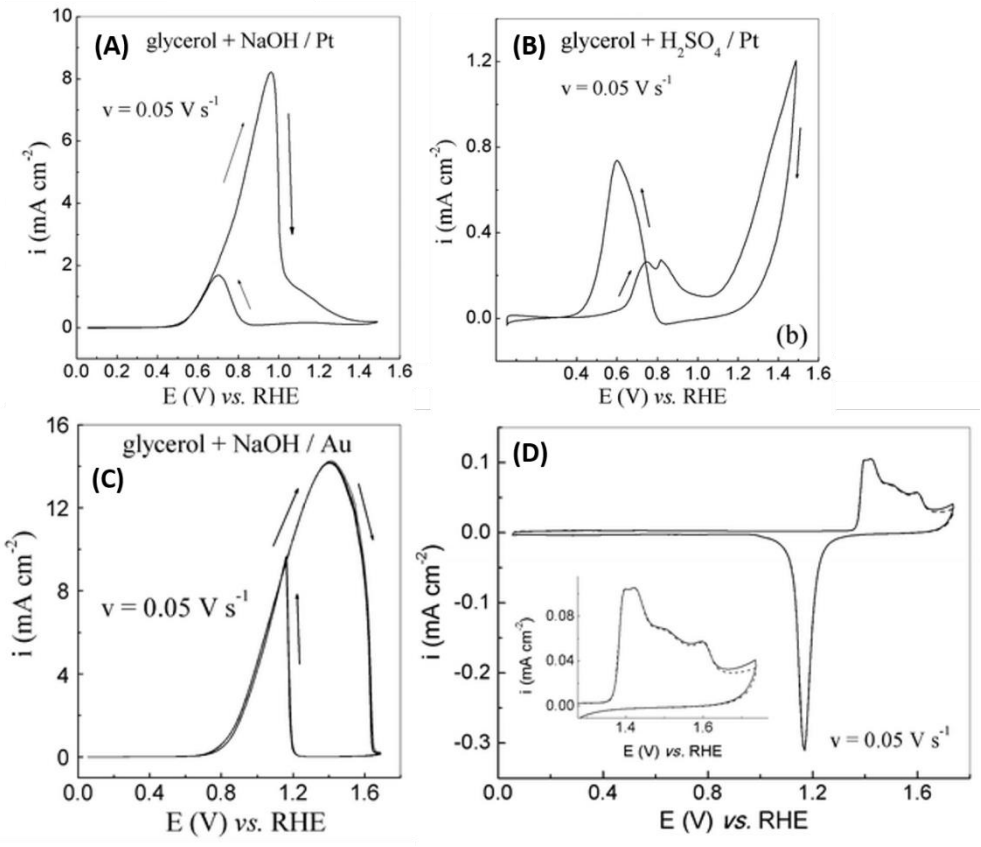


*Figure 17 Cyclic voltammograms of a polished polycrystalline* ***Pt*** *electrode in* ***(A)*** *0.1 M glycerol + 0.1 M NaOH and* ***(B)*** *0.1 M glycerol + 0.1 M $H_2SO_4$, and a polished polycrystalline* ***Au*** *electrode in* ***(C)*** *0.1 M glycerol + 0.1 M NaOH and* ***(D)*** *in 0.1 M $H_2SO_4$ (*dashed line*) and 0.1 M glycerol + 0.1 M $H_2SO_4$ (*solid line*). Adapted with permission, Janaina Fernandes Gomes et. al. Electrocatalysis, 2011, 2, 96. Copyright 2011, Springer Nature.*

The kinetics of the electro-catalytic decomposition of glycerol are faster in alkaline media (versus acidic)as the first deprotonation step is base catalysed, while the second is dependent on the catalytic activity of the substrate.[11,87]

An investigation into the electrochemical responses of Au and Pt polycrystalline electrodes towards the oxidation of glycerol (0.1 M), in both acidic ($H_2SO_4$ 0.1 M) and alkaline (NaOH 0.1 M) media was reported by Gomes and Tremiliosi-Filho, whose key results are presented in Figure 17.[88] The addition of glycerol results in increased electrochemical response from the electrodes *i.e.* greater currents being measured, barring only the Au electrode in acidic media. It is demonstrated that the Au and Pt surfaces both catalyse the reaction, with distinct oxidation peaks. The unique features assigned to both the Au and Pt electrodes provided a basis for comparison of results upon the investigation of the modified surfaces.

As the measurements for glycerol electrocatalysis were all completed in alkaline media, this is the environment that will primarily be discussed. A point to note is that while the Au and Pt activities and product distributions are affected by pH, the reaction pathways are unchanged.[85,86] In alkaline media, the intermediate of glycerol decomposition with a Pt electrode is glyceraldehyde, with the main product being glyceric acid. Glyceric acid is also the main product on an Au surface, though it is then oxidised further into glycolic and formic acid.[11] This is due to the high oxidation potentials on the gold electrode. A reaction scheme is presented in Figure 18, compiled using data from Kwon *et. al.*[85]

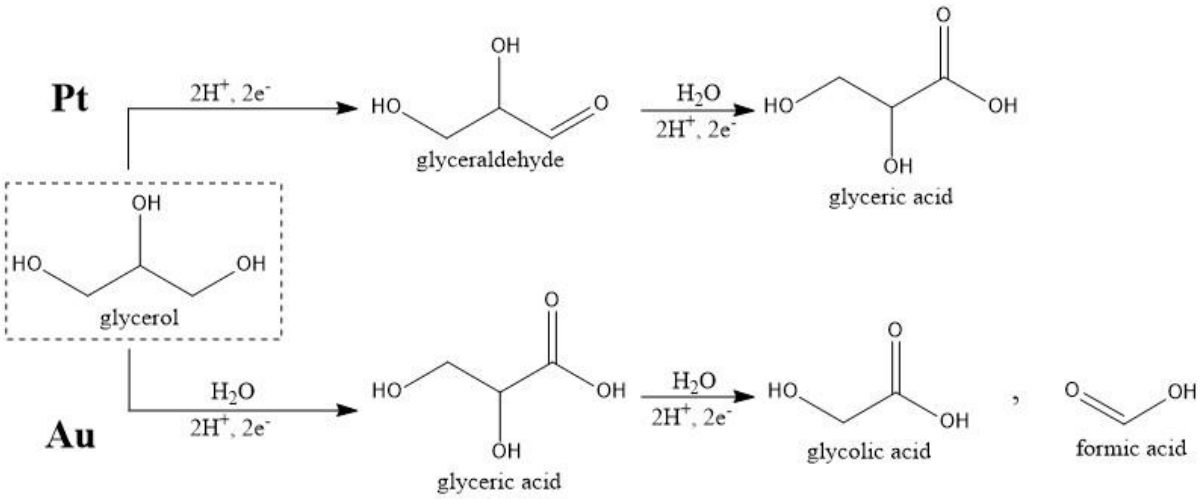


*Figure 18 A reaction scheme of the oxidation of glycerol into its intermediates and products, by Pt and Au electrodes in alkaline media.*

## 6.2 Au Electrode Response

The CV profile for a bare Au micro-electrode is shown in Figure 19. There are two distinct oxidation peaks, the primary oxidation peak in the positive scan and a secondary peak in the negative scan. As the potential increases in the positive scan direction, the adsorption of hydroxide ions begins at 0.3 $V_{RHE}$, continuing until a specific coverage of Au-OH is reached. Typically, this occurs at 0.79 $V_{RHE}$, at which point the surface has the charge specific to the adsorption of the glycerol molecule, facilitated via its $O^-$ group. The onset of glycerol adsorption is 0.8 $V_{RHE}$, coinciding with the primary oxidation peak.

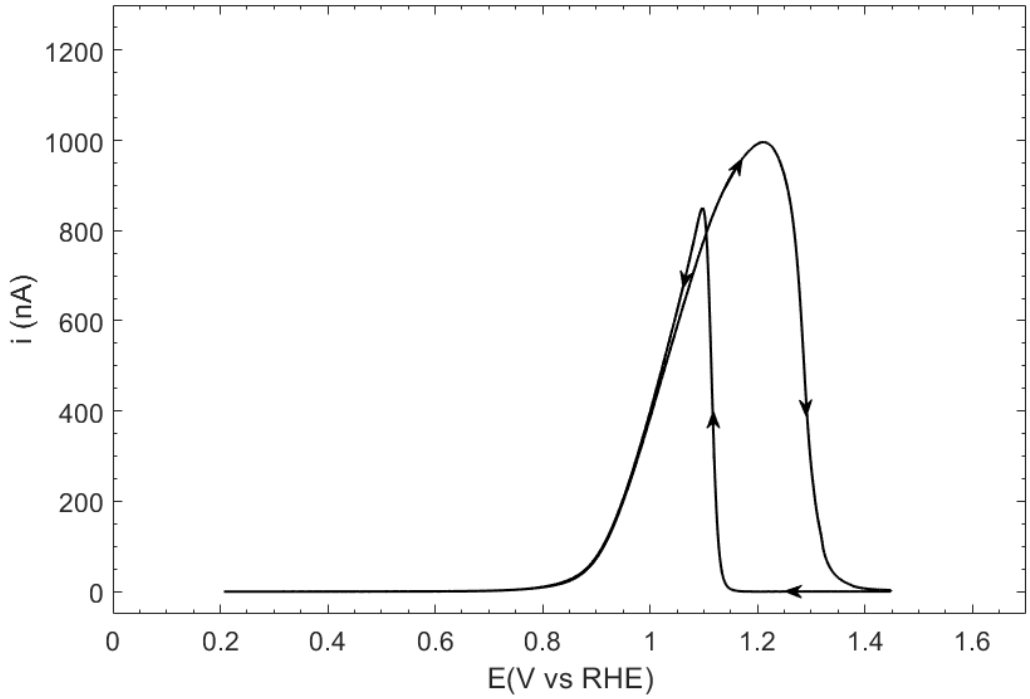


*Figure 19 Voltammetric profile of the bare Au electrode surface in 0.1 M NaOH + 0.1 M glycerol. v = 0.05 V/s*

The magnitude of the current begins to decrease at 1.2 $V_{RHE}$ and drops to approximately zero, due to the formation of an oxide monolayer (Au-O). The glycerol cannot be oxidised over this monolayer, and the process is hence inhibited at these higher potentials.

In the negative scan, reduction of the Au-O monolayer begins at 1.2 $V_{RHE}$, creating Au sites in which the glycerol can adsorb. These catalytic defect sites are especially active, and so their formation- and the subsequent adsorption of glycerol at these sites- gives a sharp peak in the voltammogram, referred to as the re-activation of the catalyst surface. The current falls once more to a zero-value as the glycerol is no longer oxidised due to the absence of OH.

## 6.3 Pt Electrode Response

The general mechanism for glycerol oxidation on Pt is the same as on the Au surface. That is not to say, however, that the electrochemical responses do not differ. According to the data presented here, Pt has an earlier onset of oxidation (~ 0.42 $V_{RHE}$) versus that of Au (~ 0.8 $V_{RHE}$), aligning with previous reports in which Pt shows greater activity towards the oxidation of glycerol when compared to Au.[85,88]

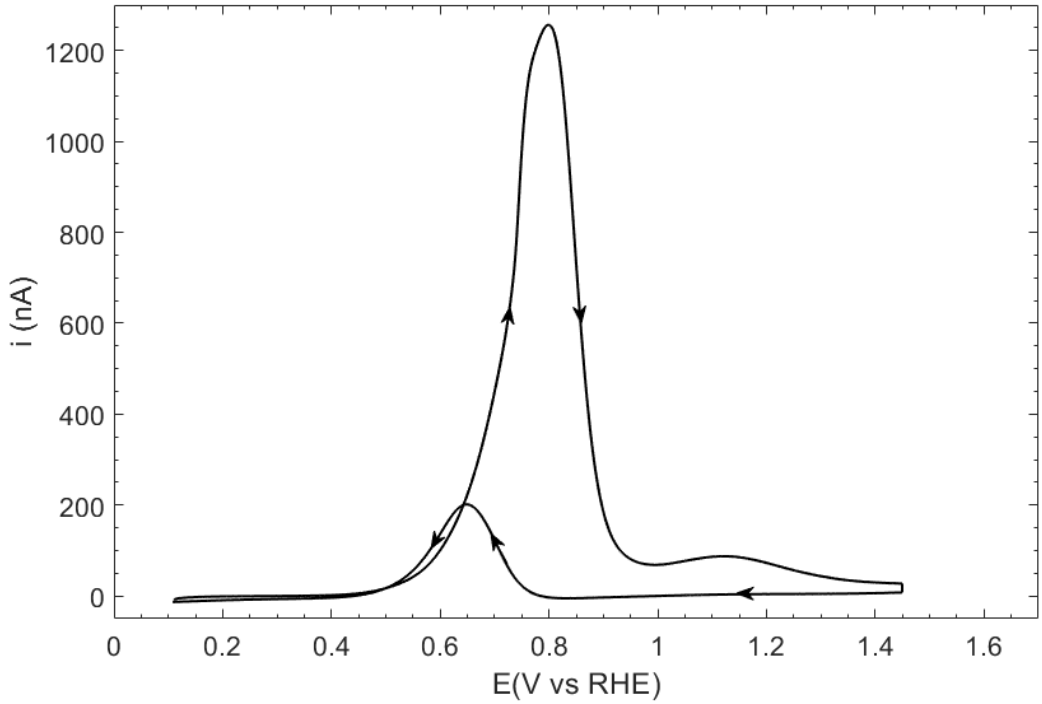


*Figure 20 Voltammetric profile of the bare Pt electrode surface in 0.1 M NaOH + 0.1 M glycerol. v = 0.05 V/s*

## 6.4 NPs on Electrode Surfaces

### 6.4.1 Au surface/PtNP

As with the experiments run in aqueous media, the electrode surfaces were modified via immersion into the relevant nanoparticle suspensions (3.1.1 Nanoparticle Synthesis). The first set of results obtained for an Au surface/PtNP system in NaOH and glycerol are presented in Figure 21. The voltammetric profile shown in orange has been recorded after surface modification. Major differences can be seen between this and the blank voltammogram (black, dotted), with perhaps the most notable being the presence of an additional peak (**a**) at *ca.* 0.8 $V_{RHE}$.

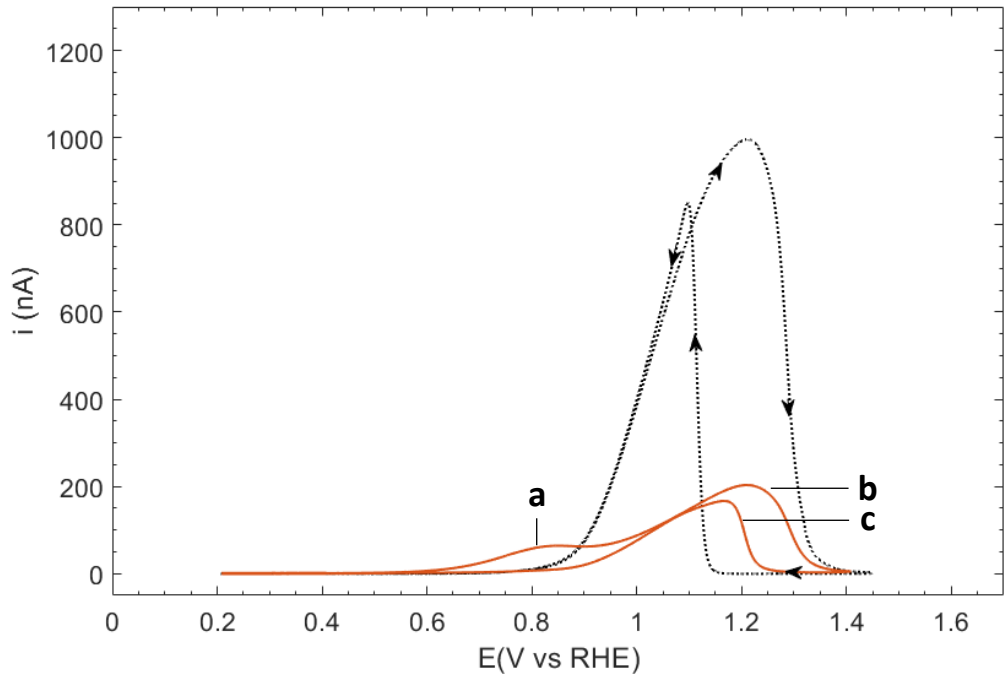


*Figure 21 Voltammetric profiles of the bare Au electrode surface (dotted black), and Au surface/PtNP (Au micro-electrode immersed in Pt NPs for 24 hours) (orange), in 0.1 M NaOH + 0.1 M glycerol. Labelled peaks correspond to: (a) characteristic Pt peak (primary oxidation), (b) characteristic Au peak (primary oxidation) and (c) characteristic Au peak (secondary oxidation). v = 0.05 V/s*

Data from the blank surface characterisation showed that the Pt electrode primary oxidation peak has an onset of 0.42 $V_{RHE}$, with a peak current at 0.8 $V_{RHE}$. The same parameters can be observed for peak **a**, with an onset of 0.45 $V_{RHE}$.

It may therefore be the case that peak **a** is due to the presence of unprotected Pt NPs on the Au surface, as the thiol capping layer diffuses onto the Au electrode surface, resulting in free Pt which is then catalytically active, resulting in the emergence of its characteristic oxidation peak. This may also be the reason for the differences in peaks **b** and **c**, in which the modified Au surface exhibits a much lower activity towards oxidation of glycerol when compared to the voltammogram of the blank electrode. This effect may be due to the blocking of surface-active sites on the electrode surface by the redistributed thiols. Blockage of these sites, as well as the general surface coverage due to the thiols presence, would lead to a lower turnover of glycerol, and hence a much lower current response intensity.

While these conclusions may be drawn from the electrochemical data, a more insightful picture of the surface behaviour may require implementation of methods *i.e.* high resolution STM imaging, as has been done in previous work.[6]

In summary, the results from this Au surface/PtNP system are as expected, as the interaction of thiol-protected Pt particles with the Au electrode surface was expected to aid in the removal of the thiol shell, due to the enthalpic and entropic driving forces. As a result, the exposed Pt would be free to participate in the catalysis of the oxidation of glycerol. Such activity was seen, due to the emergence of the Pt characteristic peak. Upon obtaining these results, the hypothesis was extended further to include the effect of 'cleaning' the modified, Au surface/PtNP electrode of the redistributed thiols, and re-immersing the electrode in the Pt NPs to explore further surface coverage. The expected outcome was a greater contribution of Pt within the voltammetric profile, while the effect on the response from the Au surface was left open to investigation.

This concept was investigated by holding the potential applied to the Au surface/PtNP at a value (0.2 $V_{RHE}$) to allow removal of thiols via reductive desorption. Holding the potential at this value for 4 minutes resulted in the maximum Au electrode response for the modified surface and no further increase even for longer holding times. The electrode was then rinsed and re-immersed into the PtNP solution for another 24 hours. The cyclic voltammograms obtained from this are presented in Figure 22.

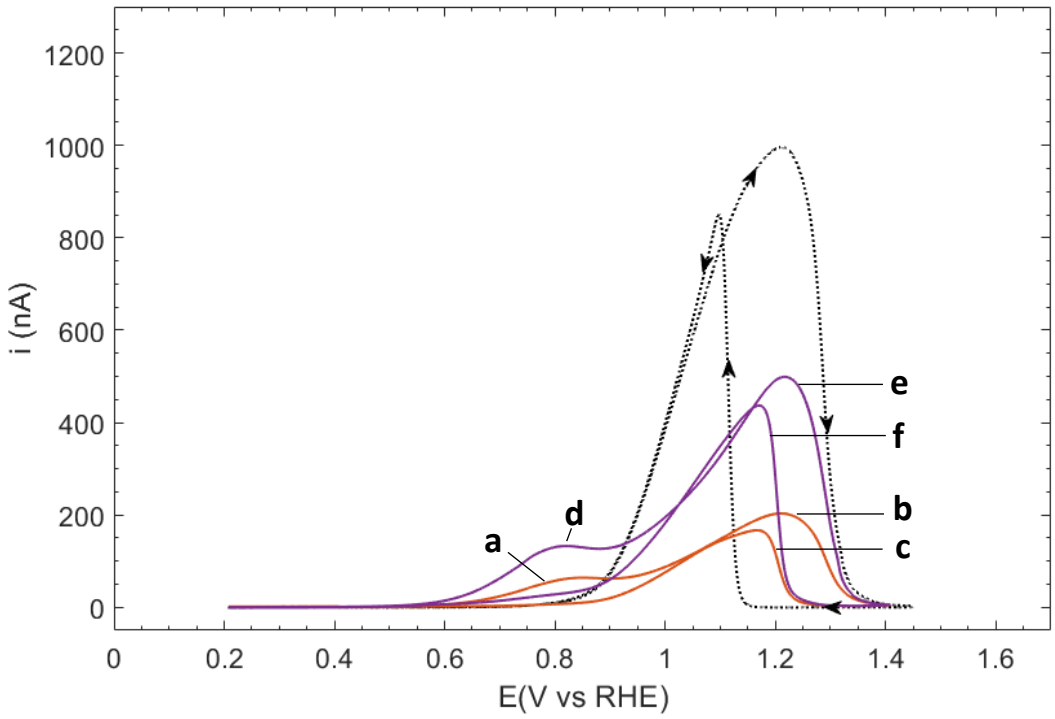


*Figure 22 Voltammetric profiles of the bare Au electrode surface (dotted black), Au surface/PtNP first immersion (orange), and Au surface/PtNP second immersion (purple) in 0.1 M NaOH + 0.1 M glycerol. Labelled peaks correspond to: (a + d) characteristic Pt peaks (primary oxidation), (b + e) characteristic Au peaks (primary oxidation) and (c + f) characteristic Au peaks (secondary oxidation). v = 0.05 V/s.*

Similar to the results presented in Figure 21, the formation of a Pt peak (**d**) was observed, though the peak grew significantly upon re-immersion. This result was in line with expectations, as the removal of redistributed thiols after the first immersion of the electrode would provide the opportunity for greater surface coverage by Pt particles upon re-immersion.

It can also be seen that the Au peaks (**e** and **f**), both primary and secondary oxidation, gave a more intense current response, despite more Pt NP having been deposited onto the surface. In between the scans of the cyclic voltammetry measurement, there was an increase in peak signals of both the Au oxidation peaks, as well as the Pt peak, for the modified surface. An example of this effect is shown in Figure 23, where results obtained from scan numbers 4, 7 and 12 are compared. The peak current measured has been plotted as a function of scan number for easy comparison in Figure 24.

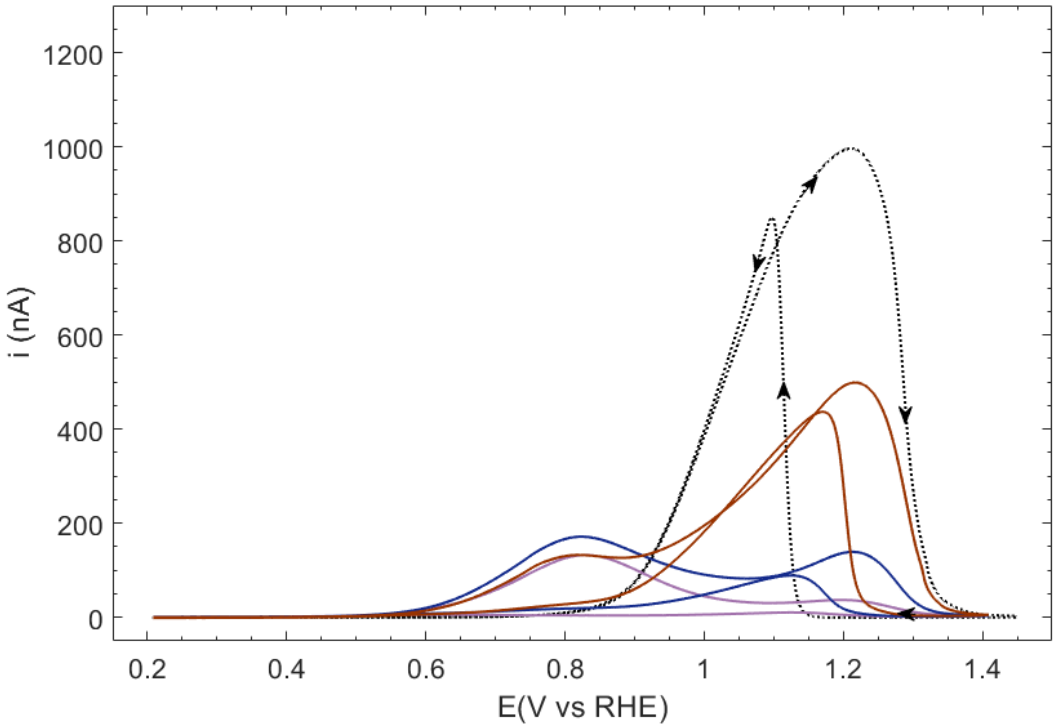


*Figure 23 Voltammetric profiles of the bare Au electrode surface (**dotted black**), Au surface/PtNP second immersion scan number: 4 (**purple**), 7 (**blue**) and 12 (**brown**) in 0.1 M NaOH + 0.1 M glycerol. v = 0.05 V/s.*

The growth of signal between scans for Pt is steep to begin with and begins to slow and plateau slightly at scan number seven, before declining and settling at a value of 132 nA. The peak growth for Au instead begins more gradually, becoming steeper at scan seven, and reaching a maximum current of 497 nA.

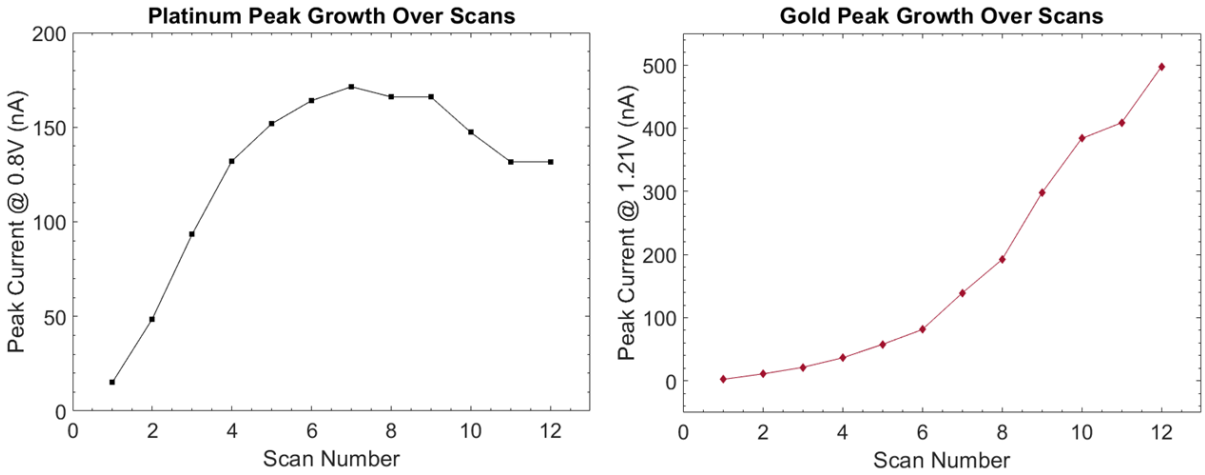


*Figure 24 Peak current plots as a function of scan number for a modified Au surface/PtNP system. 'Gold Peak' refers to the primary oxidation peak in the positive direction. For both Pt and Au peaks, the current values were taken at the potential of maximum current output, being 0.8 V and 1.2 V respectively.*

The acceleration of the growth of the Au electrode peak seemingly occurred when the Pt peak growth slowed to a decline, alluding towards a change in the Pt NP structures on the electrode surface that leads towards both:

- The exposed Pt surface decreasing
- The exposed Au surface increasing

Four possible mechanisms for the degradation of Pt NPs on electrode surfaces have been explored, and can be divided into associative (agglomeration, Ostwald ripening) and dissociative (dissolution, particle detachment) processes.[44] It has also been shown that there is often more than one degradation mechanism that takes place over the course of an electrochemical experiment, with the common finding being a change of associative to dissociative.[86] Ostwald ripening has been shown to be the dominant mechanism at low potential regions, up to 1.0 $V_{RHE}$, while dissolution of Pt particles takes place in the region above 1.15 $V_{RHE}$.[47,89]

While these mechanisms may be at play, it is difficult to determine their effect from the results, as present. An additional possibility that may be considered is the oxidative desorption of the thiols on the electrode/NP system, exposing increased amounts of both Au and Pt, leading to an increase in their respective catalytic activities, and subsequent electrochemical response. Given the relative strength of the Au-S bond, versus the Pt-S bond, it is reasonable to assume that the desorption of the thiols from the Pt surface occurs more readily than from the Au surface. Further, the timeframe of the measurement may not have been sufficient for the completion of this process, and perhaps an increased timeframe would return an Au signal of intensity equal to that recorded on the bare Au electrode surface.

### 6.4.2 Pt surface/AuNP

The results for a Pt surface/AuNP system exhibit the same trend in the presence of glycerol as was seen in the alkaline (0.1 M NaOH) environment. Upon addition of the Au NPs a lower

current response as compared to the blank Pt is seen. This could be indicative of the presence of nanoparticles, or other contaminants on the surface.

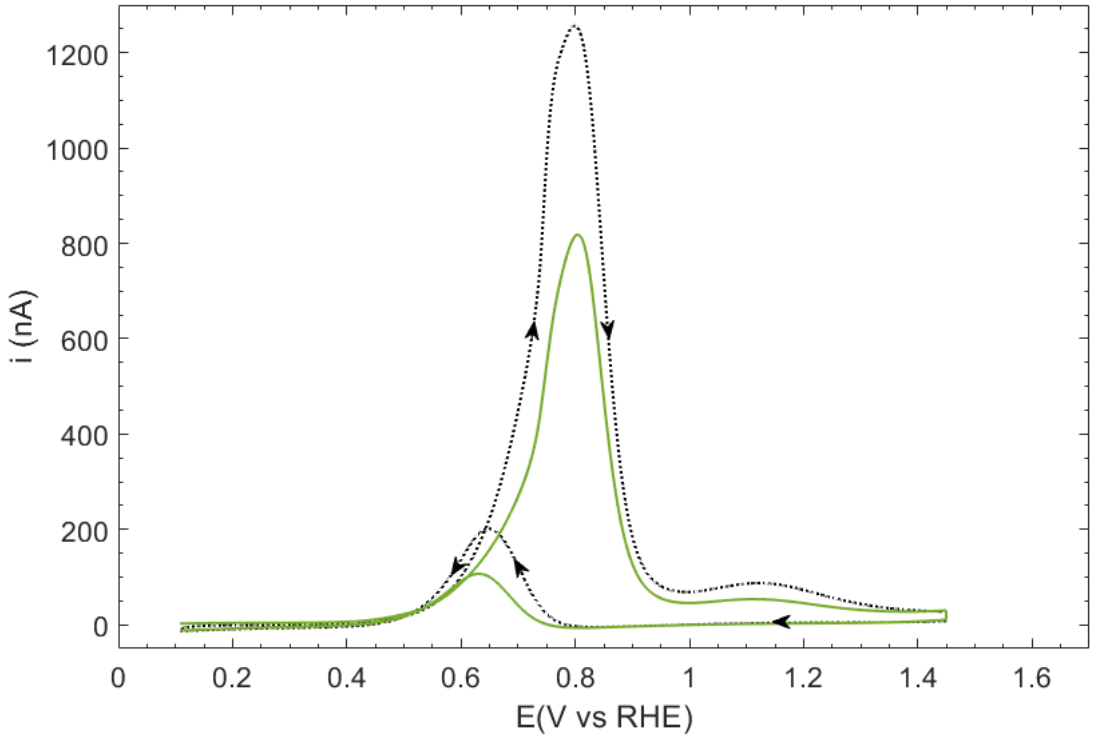


*Figure 25 Voltammetric profiles of the bare Pt electrode surface (**dotted black**), and Pt surface/AuNP (Pt micro-electrode immersed in AuNPs for 24 hours) (**green**), in 0.1 M NaOH + 0.1 M glycerol. v = 0.05 V/s*

As opposed to the measurements conducted in alkaline media (5. Electrochemistry of Au and Pt NPs in 0.1 M NaOH), the current responses of Au and Pt electrodes in the presence of glycerol are on a comparable scale. This removes the complication of any Au NP signal being 'masked'. However, no Au characteristic features are present in the voltammetric profile. Further insight is therefore needed to confirm the presence of the Au NPs on the electrode surface *e.g.* via reductive desorption of thiols, before work can be done to identify potential thiol redistribution dynamics.

## 6.5 Conclusion

Surface modification of metal surfaces with metallic, thiolated nanoparticles gave an interesting insight into their surface dynamics. Addition of Au NPs to a Pt electrode surface resulted in a lower current response of the electrode surface, with respect to the electro-catalytic decomposition of glycerol. Despite this, there were no Au characteristic features observed, and so the surface may have been (i) contaminated, likely with remaining thiols, or (ii) supporting still-protected Au nanoparticles. Further investigations are required to determine the case, for example through the reductive desorption of thiols. If Au activity is revealed after this procedure, it may be concluded that the nanoparticles remain shielded on the Pt surface, due possibly to the unfavourable energetics of Au-thiol bond breakage.

By contrast, the addition of Pt NPs to the Au electrode surface resulted in a notable change in the CV profile, as it included both Au and Pt characteristic peaks. The Pt peak showed growth upon re-immersion of the modified surface into Pt NP solution, evidencing an increase in surface coverage of the Au electrode. During the experimental measurements, an increase in Pt signal intensity with respect to the primary oxidation stage was recorded to a point, after which a plateau and decrease were observed. The Au electrode exhibited a slow increase in its signal response, which became rapid at approximately the point in the measurements at which the Pt growth decreased. This behaviour may be ascribed to the oxidative desorption of thiols, or indeed the thiol redistribution initially proposed. If the latter is the case, it may provide further evidence for the potential of the NP/surface interaction in promoting the redistribution of thiols, thereby opening avenues for further optimisation of surfaces. Further work in this respect would benefit from investigation into the Pt NPs on a non-metal surface *e.g.* glassy carbon, in order to determine if the catalytic activity features are a result only of the particles being exposed to the Au surface.

It can be difficult, however, to draw substantial conclusions on the surface dynamics of these systems, without more nuanced investigations. Electrochemical STM measurements, for example, may reveal more information regarding the specific surface effects as a result of the nanoparticles. Electrode imaging prior to, during, and after electrochemical measurements may still provide clarification as to the re-distribution of thiols into the bulk electrodes, as well as any nanoparticle degradation that may occur. The inclusion of x-ray photoelectron

spectroscopy (XPS) and other surface sensitive techniques would further provide useful insight, though this is left for future work.

# 7. References


1 F. Calle-Vallejo, M. T. M. Koper and A. S. Bandarenka, *Chem. Soc. Rev.*, 2013, **42**, 5210–5230.

2 A. Mathew and T. Pradeep, *Part. Part. Syst. Charact.*, 2014, **31**, 1017–1053.

3 M.-C. Daniel and D. Astruc, *Chem. Rev.*, 2004, **104**, 293–346.

4 H. H. Kung and M. C. Kung, *Catal. Today*, 2004, **97**, 219–224.

5 L. He, Y. Liu, J. Liu, Y. Xiong, J. Zheng, Y. Liu and Z. Tang, *Angew. Chemie Int. Ed.*, 2013, **52**, 3741–3745.

6 E. Pensa and T. Albrecht, *J. Phys. Chem. Lett.*, 2018, **9**, 57–62.

7 J. D. Aiken and R. G. Finke, *J. Mol. Catal. A Chem.*, 1999, **145**, 1–44.

8 R. Ferrando, J. Jellinek and R. L. Johnston, *Chem. Rev.*, 2008, **108**, 845–910.

9 Y.-C. Lin and G. W. Huber, *Energy Environ. Sci.*, 2009, **2**, 68–80.

10 V. Polshettiwar and R. S. Varma, *Green Chem.*, 2010, **12**, 743–754.

11 C. Coutanceau, S. Baranton and R. S. B. Kouamé, *Front. Chem.* , 2019, **7**, 100.

12 N. Mizuno and M. Misono, *Chem. Rev.*, 1998, **98**, 199–218.

13 E. Roduner, *Chem. Soc. Rev.*, 2014, **43**, 8226–8239.

14 H. S. Taylor and E. F. Armstrong, *Proc. R. Soc. London. Ser. A, Contain. Pap. a Math. Phys. Character*, 1925, **108**, 105–111.

15 J. P. Greeley, *Science (80-. ).*, 2012, **336**, 810 LP – 811.

16 Y. Lu and W. Chen, *Chem. Soc. Rev.*, 2012, **41**, 3594–3623.

17 W. Chen and S. Chen, *Angew. Chemie Int. Ed.*, 2009, **48**, 4386–4389.

18 A. A. Herzing, C. J. Kiely, A. F. Carley, P. Landon and G. J. Hutchings, *Science (80-. ).*, 2008, **321**, 1331 LP – 1335.

19 P. Rodriguez, D. Plana, D. J. Fermin and M. T. M. Koper, *J. Catal.*, 2014, **311**, 182–189.

20 C.-H. Chen, A. Halford, M. Walker, C. Brennan, S. C. S. Lai, D. J. Fermin, P. R. Unwin and P. Rodriguez, *J. Electroanal. Chem.*, 2018, **816**, 138–148.

21 G. A. Somorjai, *Adv. Catal*., 1977, **26**, 1-68.

22 H. Dong, J. Zhao, J. Chen, Y. Wu and B. Li, *Int. J. Miner. Process.*, 2015, **145**, 108–113.

23 H. A. Gasteiger, N. M. Markovic and P. N. Ross, *J. Phys. Chem.*, 1995, **99**, 8290–8301.

24 D. Y. Chung, K.-J. Lee and Y.-E. Sung, *J. Phys. Chem. C*, 2016, **120**, 9028–9035.

25 B. El Roustom, G. Siné, G. Fóti and C. Comninellis, *J. Appl. Electrochem.*, 2007, **37**, 1227–1236.

26 W. Zhou and J. Y. Lee, *Electrochem. commun.*, 2007, **9**, 1725–1729.

27 J. Suntivich, Z. Xu, C. E. Carlton, J. Kim, B. Han, S. W. Lee, N. Bonnet, N. Marzari, L. F. Allard, H. A. Gasteiger, K. Hamad-Schifferli and Y. Shao-Horn, *J. Am. Chem. Soc.*, 2013, **135**, 7985–7991.

28 J. D. Aiken, Y. Lin and R. G. Finke, *J. Mol. Catal. A Chem.*, 1996, **114**, 29–51.

29 I. I. Khan, K. Saeed and I. I. Khan, *Arab. J. Chem.*, 2019, **12**, 7, 908-931.

30 F. J. Heiligtag and M. Niederberger, *Mater. Today*, 2013, **16**, 262–271.

31 E. Pensa, E. Cortés, G. Corthey, P. Carro, C. Vericat, M. H. Fonticelli, G. Benítez, A. A. Rubert and R. C. Salvarezza, *Acc. Chem. Res.*, 2012, **45**, 1183–1192.

32 A. Verma and V. M. Rotello, *Chem. Commun.*, 2005, 3, 303–312.

33 J. Kimling, M. Maier, B. Okenve, V. Kotaidis, H. Ballot and A. Plech, *J. Phys. Chem. B*, 2006, **110**, 15700–15707.

34 P. K. Jain, I. H. El-Sayed and M. A. El-Sayed, *Nano Today*, 2007, **2**, 18–29.

35 K. M. Ø. Jensen, P. Juhas, M. A. Tofanelli, C. L. Heinecke, G. Vaughan, C. J. Ackerson and S. J. L. Billinge, *Nat. Commun.*, 2016, **7**, 11859.

36 P. Carro, E. Pensa, T. Albrecht and R. Salvarezza, *J. Phys. Chem.*, 2020, **124**, 9, 5452-5459.

37 R. Jin, *Nanoscale*, 2010, **2**, 343–362.

38 R. W. Murray, *Chem. Rev.*, 2008, **108**, 2688–2720.

39 R. S. Ingram, M. J. Hostetler, R. W. Murray, T. G. Schaaff, J. T. Khoury, R. L. Whetten, T. P. Bigioni, D. K. Guthrie and P. N. First, *J. Am. Chem. Soc.*, 1997, **119**, 9279–9280.

40 H. Qian and R. Jin, *Chem. Mater.*, 2011, **23**, 2209–2217.

41 P. B. Kettler, *Org. Process Res. Dev.*, 2003, **7**, 342–354.

42 N. K. Chaudhari, J. Joo, H. Kwon, B. Kim, H. Y. Kim, S. H. Joo and K. Lee, *Nano Res.*, 2018, **11**, 6111–6140.

43 C. M. Welch and R. G. Compton, *Anal. Bioanal. Chem.*, 2006, **384**, 601–619.

44 J. Monzó, D. F. van der Vliet, A. Yanson and P. Rodriguez, *Phys. Chem. Chem. Phys.*, 2016, **18**, 22407–22415.

45 Y. Shao-Horn, W. C. Sheng, S. Chen, P. J. Ferreira, E. F. Holby and D. Morgan, *Top. Catal.*, 2007, **46**, 285–305.

46 P. W. Voorhees, *J. Stat. Phys.*, 1985, **38**, 231–252.

47 W. Sheng, S. W. Lee, E. J. Crumlin, S. Chen and Y. Shao-Horn, *J. Electrochem. Soc.*, 2011, **158**, B1398.

48 J. C. Meier, C. Galeano, I. Katsounaros, A. A. Topalov, A. Kostka, F. Schüth and K. J. J. Mayrhofer, *ACS Catal.*, 2012, **2**, 832–843.

49 R. Sharma, S. Gyergyek, Q. Li and S. M. Andersen, *J. Electroanal. Chem.*, 2019, **838**, 82–88.

50 P. Jovanovič, A. Pavlišič, V. S. Šelih, M. Šala, N. Hodnik, M. Bele, S. Hočevar and M. Gaberšček, *ChemCatChem*, 2014, **6**, 449–453.

51 D. V Talapin, J.-S. Lee, M. V Kovalenko and E. V Shevchenko, *Chem. Rev.*, 2010, **110**, 389–458.

52 C. B. Murray, C. R. Kagan and M. G. Bawendi, *Annu. Rev. Mater. Sci.*, 2000, **30**, 545–610.

53 J. C. Azcárate, G. Corthey, E. Pensa, C. Vericat, M. H. Fonticelli, R. C. Salvarezza and P. Carro, *J. Phys. Chem. Lett.*, 2013, **4**, 3127–3138.

54 E. W. Elliott, R. D. Glover and J. E. Hutchison, *ACS Nano*, 2015, **9**, 3050–3059.

55 C. Vericat, M. E. Vela, G. Corthey, E. Pensa, E. Cortés, M. H. Fonticelli, F. Ibañez, G. E. Benitez, P. Carro and R. C. Salvarezza, *RSC Adv.*, 2014, **4**, 27730–27754.

56 L. Y. S. Lee and R. B. Lennox, *Langmuir*, 2007, **23**, 292–296.

57 J. A. Williams and C. B. Gorman, *J. Phys. Chem. C*, 2007, **111**, 12804–12810.

58 T. Laiho, J. A. Leiro and J. Lukkari, *Appl. Surf. Sci.*, 2003, **212**–**213**, 525–529.

59 M. A. Floridia Addato, A. A. Rubert, G. A. Benítez, M. H. Fonticelli, J. Carrasco, P. Carro and R. C. Salvarezza, *J. Phys. Chem. C*, 2011, **115**, 17788–17798.

60 J. Feng, D. Chen, A. S. Sediq, S. Romeijn, F. D. Tichelaar, W. Jiskoot, J. Yang and M. T. M. Koper, *ACS Appl. Mater. Interfaces*, 2018, **10**, 9532–9540.

61 F. E. Kruis, H. Fissan and A. Peled, *J. Aerosol Sci.*, 1998, **29**, 511–535.

62 H. G. Scheibel and J. Porstendo¨rfer, *J. Aerosol Sci.*, 1983, **14**, 113–126.

63 C. Jackson, O. Conrad and P. Levecque, *Electrocatalysis*, 2017, **8**, 224–234.

64 J. Feng, X. Guo, N. Ramlawi, T. V Pfeiffer, R. Geutjens, S. Basak, H. Nirschl, G. Biskos, H. W. Zandbergen and A. Schmidt-Ott, *J. Mater. Chem. A*, 2016, **4**, 11222–11227.

65 J. Turkevich, *Gold Bull.*, 1985, **18**, 86–91.

66 M. Brust, M. Walker, D. Bethell, D. J. Schiffrin and R. Whyman, *J. Chem. Soc. Chem. Commun.*, 1994, **7**, 801–802.

67 E. G. Castro, R. V Salvatierra, W. H. Schreiner, M. M. Oliveira and A. J. G. Zarbin, *Chem. Mater.*, 2010, **22**, 360–370.

68 P. Rodriguez, F. D. Tichelaar, M. T. M. Koper and A. I. Yanson, *J. Am. Chem. Soc.*, 2011, **133**, 17626–17629.

69 M. J. Lawrence, A. Kolodziej and P. Rodriguez, *Curr. Opin. Electrochem.*, 2018, **10**, 7-15.

70 A. I. Yanson, P. Rodriguez, N. Garcia-Araez, R. V Mom, F. D. Tichelaar and M. T. M. Koper, *Angew. Chemie Int. Ed.*, 2011, **50**, 6346–6350.

71 Y. I. Yanson and A. I. Yanson, *Low Temp. Phys.*, 2013, **39**, 304–311.

72 A. I. Yanson, P. V Antonov, Y. I. Yanson and M. T. M. Koper, *Electrochim. Acta*, 2013, **110**, 796–800.

73 P. K. Jain, X. Huang, I. H. El-Sayed and M. A. El-Sayed, *Plasmonics*, 2007, **2**, 107–118.

74 M. V Sujitha and S. Kannan, *Spectrochim. Acta Part A Mol. Biomol. Spectrosc.*, 2013, **102**, 15–23.

75 X. Huang and M. A. El-Sayed, *J. Adv. Res.*, 2010, **1**, 13–28.

76 Z. L. Wang, *J. Phys. Chem. B*, 2000, **104**, 1153–1175.

77 DoITPoMS and University of Cambridge, Transmission Electron Microscopy, https://www.doitpoms.ac.uk/tlplib/tem/index.php, (accessed 10 November 2019).

78 S. Hebie, Y. Holade, K. Servat, B. K. Kokoh and T. W. Napporn, *IntechOpen*., 2016, 101-130.

79 L. D. Burke and P. F. Nugent, *Gold Bull.*, 1997, **30**, 43–53.

80 N. Elgrishi, K. J. Rountree, B. D. McCarthy, E. S. Rountree, T. T. Eisenhart and J. L. Dempsey, *J. Chem. Educ.*, 2018, **95**, 197–206.

81 S. Hebié, T. W. Napporn, C. Morais and K. B. Kokoh, *ChemPhysChem*, 2016, **17**, 1454–1462.

82 D. Zhan, J. Velmurugan and M. V Mirkin, *J. Am. Chem. Soc.*, 2009, **131**, 14756–14760.

83 P. Daubinger, J. Kieninger, T. Unmüssig and G. A. Urban, *Phys. Chem. Chem. Phys.*, 2014, **16**, 8392–8399.

84 T. Bürgi, *Nanoscale*, 2015, **7**, 15553–15567.

85 Y. Kwon, K. J. P. Schouten and M. T. M. Koper, *ChemCatChem*, 2011, **3**, 1176–1185.

86 M. Simões, S. Baranton and C. Coutanceau, *ChemSusChem*, 2012, **5**, 2106–2124.

87 Y. Kwon, S. C. S. Lai, P. Rodriguez and M. T. M. Koper, *J. Am. Chem. Soc.*, 2011, **133**, 6914–6917.

88 J. F. Gomes and G. Tremiliosi-Filho, *Electrocatalysis*, 2011, **2**, 2, 96.

89 A. A. Topalov, I. Katsounaros, M. Auinger, S. Cherevko, J. C. Meier, S. O. Klemm and K. J. J. Mayrhofer, *Angew. Chem. Int. Ed. Engl.*, 2012, **51**, 12613–12615.